ESTIMATION OF TENSION IN STAY CABLES AT THE INDIAN RIVER INLET BRIDGE USING FREQUENCY BASED METHODS

by

Kent S. Davidson

A thesis submitted to the Faculty of the University of Delaware in partial fulfillment of the requirements for the degree of Master of Civil Engineering

Summer 2013

ESTIMATION OF TENSION IN STAY CABLES AT THE INDIAN RIVER INLET BRIDGE USING FREQUENCY BASED METHODS

by

Kent S. Davidson

Approved: ______________________________
Harry W. Shenton III, Ph.D.
Professor in charge of thesis on behalf of the Advisory Committee

Approved: ______________________________
Harry W. Shenton III, Ph.D.
Chair of the Department of Civil and Environmental Engineering

Approved: ______________________________
Babatunde Ogunnaike, Ph.D.
Dean of the College of Engineering

Approved: ______________________________
James G. Richards, Ph.D.
Vice Provost for Graduate and Professional Education

ACKNOWLEDGMENTS

I would like to first and foremost thank Dr. Shenton for not only giving me the opportunity to continue my studies but giving me the opportunity to work on an incredible project that will contribute greatly to the University of Delaware, DelDOT, and the general engineering community. I would also like to thank Dr. Shenton for his guidance and friendship over the past four years of working with him on this project, and I am grateful to have him as an advisor and friend.

I would like to thank the members of the IRIB discussion group for their insight and help in getting my research and thesis complete including: Dr. Chajes, Pablo Marquez, and Hadi Al-Khateeb. I would like thank my fellow grad students and friends for helping me get to this point, without everybody it would have been much harder to be here.

I would like to especially thank Gary Wenczel for everything that he did in helping me accomplish this research. Gary made the long twelve to fourteen hour days seem like only minutes and he was very vital in helping me survive some of those long work days. Although not a graduate student, I will always consider Gary my best friend in graduate school, the amount of time and laughs we spent together I will never forget. I truly appreciate every minute we got to spend on the bridge and I thank you sincerely as a friend, I would not have finished graduate school without you.

Finally I would like to thank my parents and family for giving me skills, opportunities, and blessings to get to this point in my life. Had it not been for your drive, persistence, and support I would not be where I am. I love you all.

TABLE OF CONTENTS

Appendix

LIST OF TABLES

LIST OF FIGURES

LIST OF EQUATIONS

ABSTRACT

The purpose of this study is to prove that using fiber optic accelerometers in conjunction with dynamic cable theory can be used to measure the tension in eleven cable stays on the Indian River Inlet Bridge. The idea being that the accelerations from the cables vibrations have embedded frequencies that can be extracted using spectral density techniques and processed using MATLAB script files. After the accelerations are processed and the frequencies are extracted and organized, the cables tension can be calculated using dynamic cable theory and cable properties from the bridge design specifications. This study uses two types of vibrations, plucked vibrations and ambient vibrations, to test the sensors abilities to get acceleration time history data that is capable of producing frequency peaks. The results show that the sensors excel in recording accelerations from ambient and plucked vibrations. Also, the results show that the basic dynamic cable equation is a fast and accurate method for calculating cable tensions. It is found that the tensions found in the plucked vibration tests are 0.87 and 0.98 of the final hydraulically measured tensions. This study provides supporting evidence into using in situ accelerometers as a practice for monitoring the long term health of cables on the Indian River Inlet Bridge and other cable stayed bridges.

Chapter 1

INTRODUCTION

With the advance of technology structures have become increasingly complex in nature due to advances in software and construction methods. As the complexity of these structures increases, the need for fast and reliable structural monitoring systems and equipment has come about. Assessing structural health is imperative to the longevity of any structure; the sooner a structural issue is detected the faster a repair can be made.

1.1 Motivation and Background

A recent trend in bridge design has been a move to long span cable stayed bridges where the bridge main span is held up by a system of cables that is connected to one or more towers, also known as pylons, to support the bridge deck. The cables in these bridges carry the weight of the deck and all traffic loads to the pylons and subsequently into the foundation. The cables carry no compression and are always in tension. Knowing the forces in the stay cables is one way of monitoring the "health" or condition of the cables, and therefore the health of the bridge. However, the force in a stay cable is hard to measure directly. Direct methods involve using a force transducer or a hydraulic jack to measure the tension in the stay, a process which is difficult and time consuming.

Because this process is too arduous, easier methods for indirectly estimating the tension have been developed based on measuring the vibration of the stay. Basic taut cable theory provides a relationship between the tension in a stay cable and its natural frequencies. Accelerometers attached to a stay can be used to measure the vibration of the cable. The accelerometers measure the acceleration in the cables movement, from which, using classical spectral analysis techniques, the natural frequencies can be extracted and the tensions can be estimated. If the estimated tensions are greatly different than expected this could indicate some problem with the cables.

1.2 Overview of the Bridge

The focus of this study was on the Indian River Inlet Bridge, located on Delaware Route 1 (DE 1) and spanning the Indian River Inlet. This bridge connects Rehoboth Beach and Bethany Beach and is a major travel corridor between Dover, Delaware and Ocean City, Maryland. Figure 1.1 is an aerial photograph of the bridge.

Figure 1.1: Indian River Inlet Bridge

The bridge is a cable stayed design with 152 stay cables attached into four pylons, the highest of which rises about 250 feet above the inlet. The bridge consists of four twelve foot travel lanes, two northbound and two southbound, ten foot shoulders on either side of the bridge, and a ten foot wide pedestrian walkway on the east side of the bridge. Also, on the east side is a sand bypass system mounted to the edge girder at deck level to move sand from the south to the north side of the inlet. In total the bridge has a length of 2,600 feet, a main span of 950 feet, and is approximately 110 feet wide. The bridge was constructed under a design-build contract by the team of AECOM and Skanska USA Civil Southeast.

1.3 Basic Cable Dynamics and Taut Cable Theory

Unlike systems modeled with a finite number of degrees of freedom, continuous systems are represented by the summation of an infinite series of all the mode shapes in the system. In the study of continuous dynamic systems the thin taut cable is one of the first systems that are discussed. Although continuous systems are described as the infinite summation of all modes in the systems, most continuous system vibrations are dominated by the first few modes in the series. The first of these modal frequencies is known as the fundamental frequency and usually elicits the largest response.

The governing equation of motion for a continuously vibrating cable as seen below in (1.1) (Zui et. al 1996), relates the displacement to the cable's characteristics.

$$T\frac{\partial^2 w}{\partial x^2} - m\frac{\partial^2 w}{\partial t^2} + h\frac{d^2 w}{dx^2} - EI\frac{\partial^4 w}{\partial x^4} = 0 \tag{1.1}$$

In this 4^{th} order equation, w is the cable displacement, T is the cable tension, m is the linear mass per unit length of the system, h is additional tension from vibration, L is the length of the cable, and EI is the flexural rigidity of the cable. For large cables with thick cross sections the flexural element is quite important in estimating the cable tension (Triantafyllou and Grinfogel 1986). The additional tension from vibration, h, is relevant if the cable experiences large sag (Zui et al 1996). The partial derivatives are for displacements related to the spatial and time domains, x is the spatial component and t is the time component of displacements. Figure 1.2 shows the cable properties on a sample cable that mimics that of the cables being monitored.

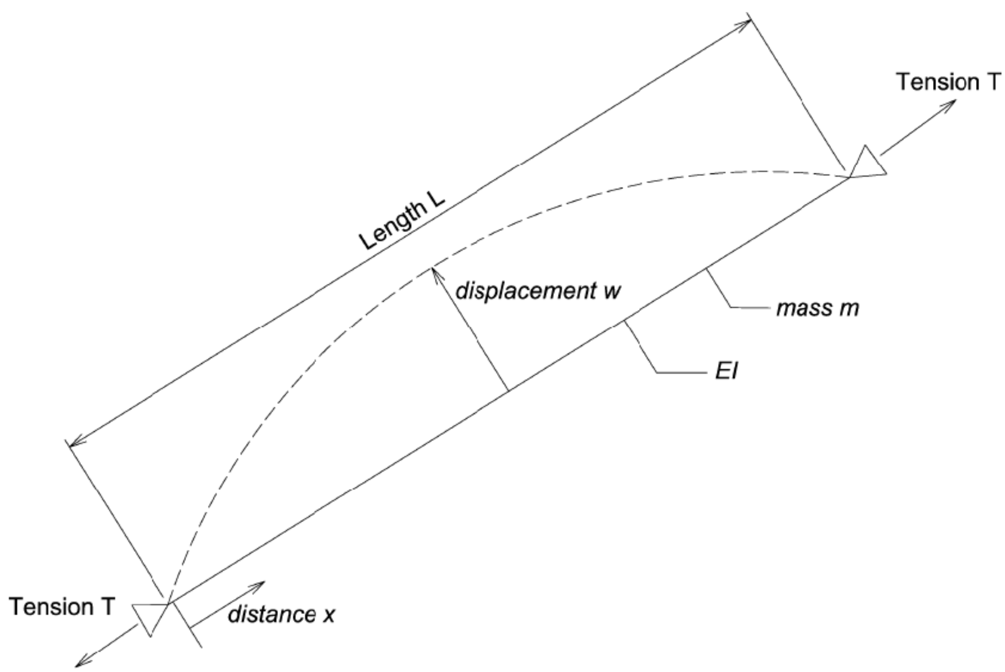

Figure 1.2: Variable Designation of Cables

For thin taut cables, the most basic of vibrating dynamic cables, neglecting the flexural stiffness of the cable, additional tension due to the cable vibration, and sag, the equation of motion (1.1) reduces to:

$$T\frac{\partial^2 w}{\partial x^2} = m\frac{\partial^2 w}{\partial t^2} \qquad (1.2)$$

Equation (1.2) is the fundamental partial differential equation for a thin taut vibrating cable and can be extended too many different applications. The equation is simplified to relating the cable's tension to the linear mass of the system by way of the partial differential equation. The solution to this equation, found in Dynamics of Structures (Chopra 2007), can be used to estimate the tension of a cable through the frequency of vibration. Solving the eigenvalue problem associated with (1.2) yields the equation for the natural frequencies of the cable:

$$f_n = \frac{n}{2L}\sqrt{\frac{T}{m}} \qquad (1.3)$$

Solving (1.3) for the tension yields

$$T = 4mL^2\left(\frac{f_n}{n}\right)^2 \qquad (1.4)$$

Equation (1.4) relates the natural frequency f_n, to the tension T, mass m, mode number n, and cable length L. In this equation the linear mass and length can be assumed known from design specifications or the as-built condition. By measuring the frequency and knowing the mode number, the tension in the stay can be easily estimated. Equation (1.4) will be used to estimate the tension in the cables on the Indian River Inlet Bridge. More refined methods for calculating cable tension will be discussed in Chapter 2 but the method proposed in taut cable theory is practical for the purposes of this research.

1.4 Research Objectives

As previously stated, the need to monitor the structural capacity of a structure is essential to a long bridge life; using a system that is constantly running is ideal for the monitoring process. Cable tension cannot be estimated directly therefore accelerometers mounted on the cable casings can measure the acceleration of movement of the cable from an excitation. Using established spectral techniques, the accelerations can be converted into the frequency domain. In conjunction with (1.4), design specifications, and the fundamental frequencies, cable tensions can be quickly estimated. The objective of this research is to estimate specific cable tensions from measured fundamental frequencies and automate a computer program that can find those frequencies from a data set and automatically estimate the tension. The stay frequencies, and therefore tensions, were estimated using two different approaches: first, based on measurements from a "pluck" test in which the stay was manually set in motion and then allowed to vibrate freely, and second, based on measurements of ambient vibrations of the stays.

1.5 Thesis Outline

This thesis will provide insights into tension estimations of the cables on the Indian River Inlet Bridge. A brief summary of cable dynamics and taut cable theory has been presented which will be the foundation of this research. First, in Chapter 2 a review of earlier research in the area of cable dynamics and cable tension estimation is presented. In Chapter 3, the data acquisition system, sensors, computer methods, and bridge elements will be described in greater detail. Presented in Chapter 4 are the results and analysis of both pluck vibration tests. Chapter 5 provides results and analysis into the ambient vibration data that was gathered. Also, in Chapter 5 signal aliasing is presented and discussed. Finally, in Chapter 6 general analysis and conclusions are given. Furthermore problems associated with the sensors and possible future research with the system is explored.

Chapter 2

LITERATURE REVIEW

The equations for estimating tension can both be complex like in (1.1) and simple like in (1.2). This following section will be used to explore the understanding of cable dynamics more in depth than the equations developed in Chapter 1.

In 1974, H. M. Irvine and T. K. Caughey published a paper on the linear theory of vibrations of suspended cables. The linear theory they develop is based on the partial differential equation in (1.1). From their findings they developed a relationship between cable geometry and elasticity, denoted as λ^2, defined below in (2.1), which was also readily adopted by other researchers (Irvine and Caughey 1974).

$$\lambda^2 = (\frac{8d}{L})^2 * \frac{1}{\frac{HLe}{EA}} \tag{2.1}$$

In the equation for λ^2, the *d* is the sag in the parabolic cable, *H* is the tension in the cable, L_e is the horizontal chord length of the cable, and *EA* represents the cables cross sectional stiffness. The λ^2 value is used by Irvine and Caughey to describe a phenomenon where the first frequency of vibration is actually higher than the second frequency. For the cables that are being monitored at the Indian River Inlet Bridge the λ^2 values are all very low, less than 0.2. The theory behind the cross over phenomenon is that for certain values of λ^2, the first natural frequency of vibration will actually be higher than the second natural frequency. For values up to $\lambda^2 = 4\pi^2$ they observe that there is no crossover of modes, for values over $\lambda^2 = 4\pi^2$ a cross over occurs at the 1st and 2nd mode of vibration (Irvine and Caughey 1974). In the case where $\lambda^2=4\pi^2$ the 1st two frequencies of vibration will adopt characteristics of the both the 1st and 2nd mode and create what Irvine and Caughey describe as a "hybrid" mode. Avoided crossings of modes, where the modes are close to crossing but don't, usually only occur in cases where a cable is not tensioned adequately in relation to its cross sectional properties and length. Their research also assumes that the cable is completely inextensible in the axial direction, meaning that the cable is not allowed to extend and it eliminates axial forces due to cable extension. The cross over phenomenon that Irvine and Caughey found is important for describing horizontal taut cable behavior.

Triantafyllou and Grinfogel expanded on the horizontal equations developed by Irvine and Caughey in 1986. They stated that the equations developed by Irvine and Caughey did not accurately represent inclined cables. The two instead used the horizontal taut cable as a limiting factor when developing their equations (Triantafyllou and Grinfogel 1986). They decided to ignore the effects of the cables bending stiffness and the excitation of elastic waves in the cable. Since the horizontal cable condition was used as a boundary, the equation can be reduced to a simple horizontal cable equation when the inclination angle is zero (Triantafyllou and Grinfogel 1986). They show this by reproducing the results of a "double solution for $\lambda=n\pi$, which causes a "crossover" phenomenon" (Triantafyllou and Grinfogel 1986). This simply means that for certain conditions the crossover will happen for horizontal cables. Their main findings deal with accurately predicting when crossovers will occur and quantifying the dynamic tension. Their first finding is that "inclined cables have different properties from horizontal cables in that a crossover does not occur and hybrid modes are formed" (Triantafyllou and Grinfogel 1986). Their second large finding is at these stated hybrid modes where the 1st and 2nd modes are similar a large "dynamic tension amplification" can be observed (Triantafyllou and Grinfogel 1986). Although the cables used in the Indian River Inlet Bridge study are inclined, the taut string equation is still more accurate than the equations from this study.

In the previous discussions the flexural rigidity and sag are neglected in the developed equations for finding cable tensions. In 1996 Zui et al. stated that most equations to that point did not "yield good results when the cable is not slender or not sufficiently tensioned". They developed equations that consider sag, flexural rigidity, inclination angle, as well as other important cable parameters; their idea was to cover a wider range of cable conditions. By using two variables Γ and ξ they are able to categorize any cable and its sag conditions in one of three ranges of equations for estimating cable tensions (Zui et al. 1996). The variable Γ is calculated to find a range in which the cable and its sag conditions fall into (Zui et al. 1996). Calculating the ξ variable yields one of the equations in the range found from Γ (Zui et al. 1996). They find that there equations align well with a finite element model that they developed for their parametric study. The formulas they develop "are in algebraic form [and] cable forces are calculated directly from natural frequencies", they continue saying that "the formulas are applicable for any cable independent of length and internal force of the cable" (Zui et al 1996). For very long cables that may be hard to get a large natural response from the 1st or 2nd mode, "a formula is presented by using natural frequencies of high-order modes obtained from stationary micro vibrations" (Zui et al 1996). They show that their equation are applicable for any cable and cable condition using the first few fundamental frequencies or higher-order frequencies when necessary.

Expanding on research conducted by Irvine, Caughey, Triantafyllou, and Grinfogel, in 1998 J.C. Russel and T.J. Lardner used experimentation to determine the frequencies and tensions for cables. They address the avoided crossings issue by citing the findings of Triantafyllou and Grinfogel in the assumption that for inclined cables there is no one point where symmetric and asymmetric frequencies will cross but exhibit properties as a hybrid mode. Their experimental set up uses a guy wire outfitted with small lead weights spaced evenly over the length of the 38.25 foot cable. At the base of the cable a force transducer was attached to measure the horizontal force in the cable, accelerometers were attached near the base to measure the acceleration of the in plane motion (Russell and Lardner 1998). Their results show that their model aligns with Triantafyllou and Grinfogel equation for predicted natural frequencies of inclined cables. Also, they show that the avoided crossing phenomenon occurs with higher values of λ^2 further confirming the idea that avoiding crossing will occur with low tension in (2.1) (Russell and Lardner 1998). Other than their results confirming the avoided crossings theory, they also were able to calculate the natural frequencies with an average of only 0.7% deviation from predicted natural frequencies (Russell and Lardner 1998). From the measured natural frequencies they were able to estimate the base tension of a cable within 3% of the actual tension in the force transducer (Russell and Lardner 1998).

In 2007 a comparative performance study was conducted on the various methods used to estimate cable tension (Kim et al 2007). The methods that were evaluated in the study were string theory as in the solution to (1.2), an equation that's solution expands upon (1.3) adding a component of flexural rigidity, the third is considered to be “modern cable theory” which is the equation developed by

Triantafyllou and Grinfogel in 1986, cable tension equation developed by Zui et al in 1996, a linear regression model, and a self adjusting system identification method that uses a finite element model developed by the author. The bridge that the data was gathered from is the Seohae Bridge near Seoul Korea, where two cables from the bridge were sampled with horizontal spans of 200 meters and 131 meters (Kim el al 2007). Their results show that a linear regression and the self adjusting identification system produced the most consistent results over the range of modes. Out of the non-iterative processes the string theory equation was the most accurate at getting a consistent tension in the frequency range. The modern cable theory equation and equations developed by Triantafyllou and Grinfogel represent the upper and lower bounds of the tension ranges for a given cable (Kim et al 2007). Their findings show that the string theory equations vary from less than 2% for all cables analyzed (Kim el al 2007). This study shows that the simple taut cable approach from (1.4) is a better estimator of tension for cables that are sufficiently tensioned, as in most cables on cable stayed bridges, and other more complex methods do not necessarily need to be used.

Chapter 3

SPECIFICS OF BRIDGE AND MONITORING SYSTEM

This chapter will be used to further discuss in detail aspects concerning the cables on the bridge, data acquisition system, and accelerometers used on the cables to collect data. Also, the computer analysis methods will be explained in more detail.

3.1 Cable Specifications

3.1.1 Bridge Layout

A diagram showing an elevation view of the entire bridge is shown below in Figure 3.1 (Figure 3.1 looks at the bridge from the east side with north being to the right). The cables 101-119 are to the south of pylon 5 and 201-219 to the north. Cables 301-319 are to the south of pylon 6 and 401-419 are to the north. The numbering is sequential with the longer, higher numbered cables being the furthest from the pylon, e.g., 119, and the shorter, lower numbered cables being closest to the pylons, e.g. 101.

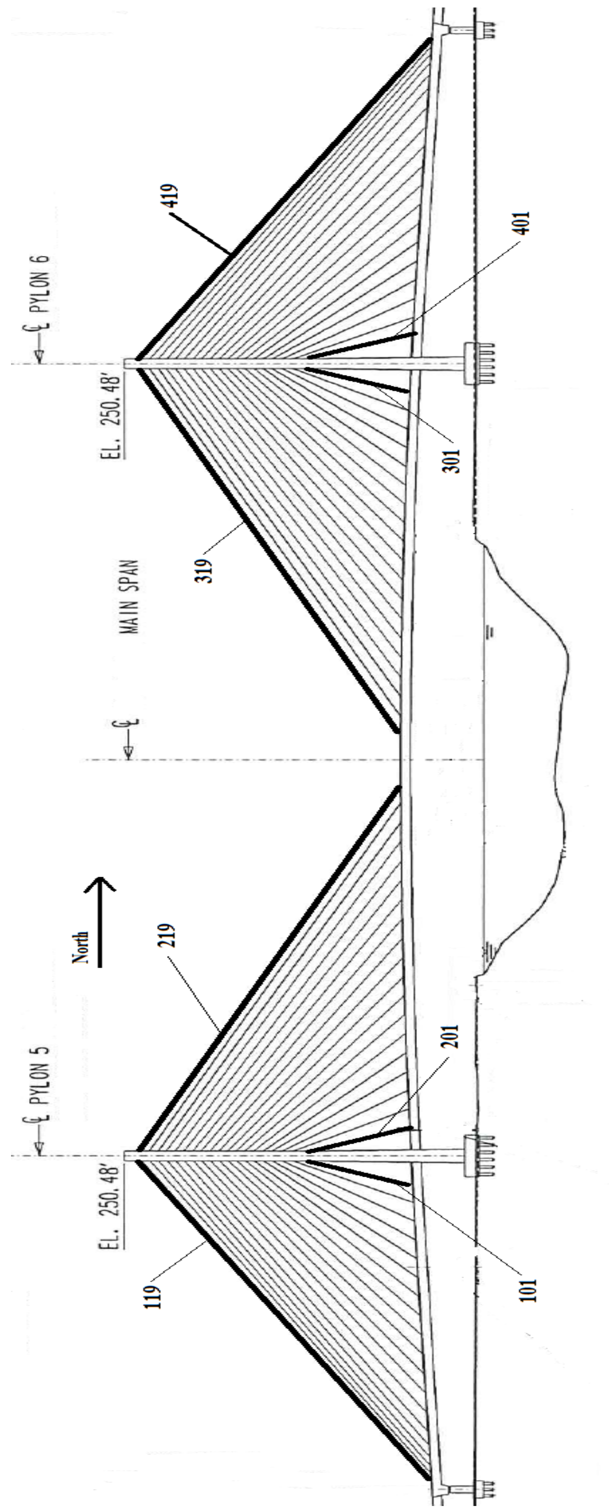

Figure 3.1: Elevation View of Indian River Inlet Bridge

3.1.2 Cable Specifications

Inside the cable sheath are different numbers of strands threaded through collars at the deck level and in the pylons. The number and arrangement of the strands vary in the cables. Each strand is made of seven wire weldless low relaxation grade 270 ksi steel in compliance with ASTM standard A416 with a minimum ultimate capacity of 62.8 kips (AECOM Construction Drawing). The cable system was anchored to the pylons as shown below Figure 3.2.

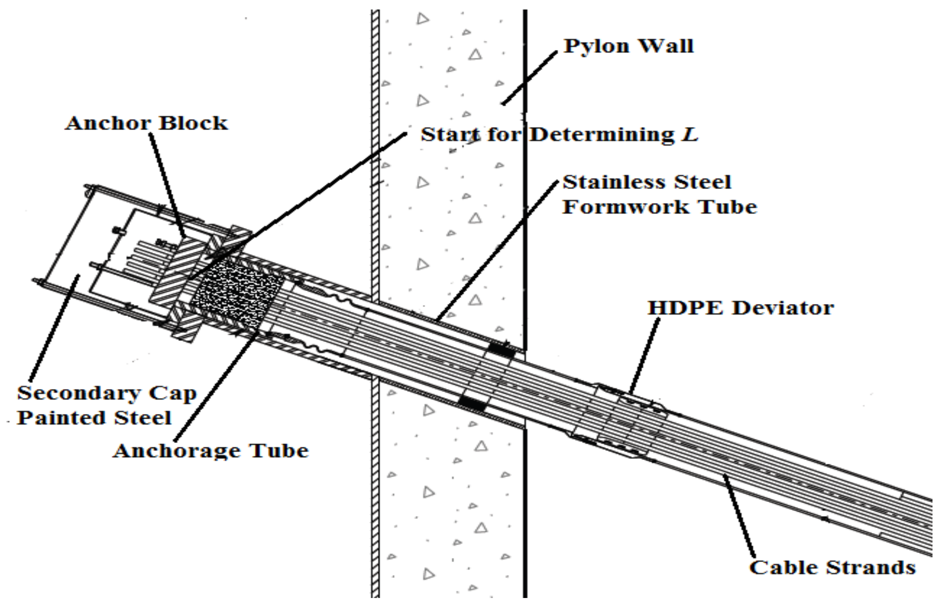

Figure 3.2: Anchorage System At Pylon Level

The cables are threaded from the inside of the pylon (left of the drawing), into the anchor block and then pushed to the outside of the pylon wall (right of the drawing), then through the anchorage tube. The cables are held in place by a collar in the anchor block which is supported by the anchorage tube. A steel cap seals the anchorage system and any voids in the system are filled with wax, this is to prevent any corrosion of the cables from moisture inside the pylon. The cable anchorage system is inside the pylon and is accessible via a steel platform that is located at every cable level. Note that there is no damper installed at the top cable anchorage system. At the deck level the cables are anchored as shown in Figure 3.3.

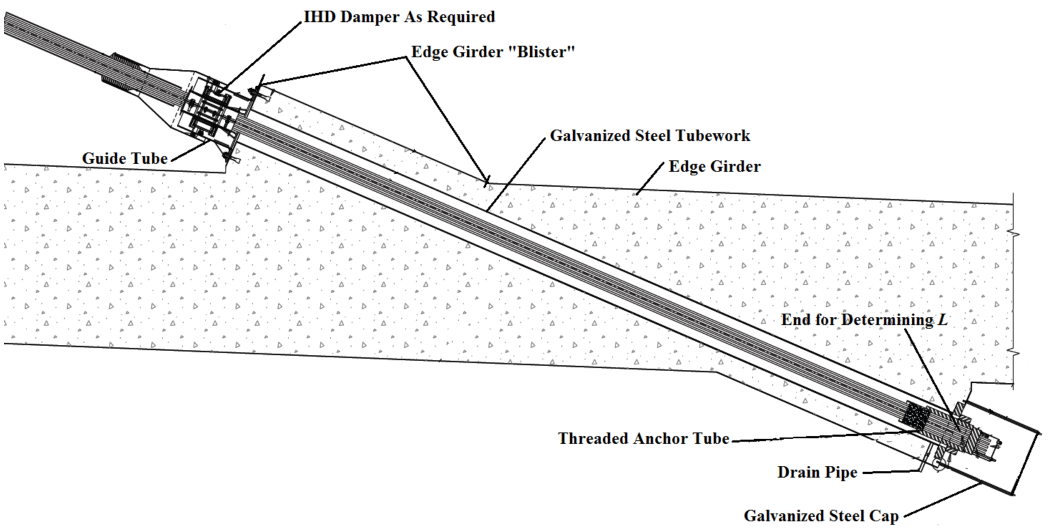

Figure 3.3: Cable Anchorage System at Deck Level

The cable strands enter the edge girder at the edge girder blister, which is at deck level, through the guide tube which guides the strands into the steel tube that is cast into the edge girder. Wrapped around the cables above the guide tube is a hydraulic damper that is shown in more detail in Figure 3.4.

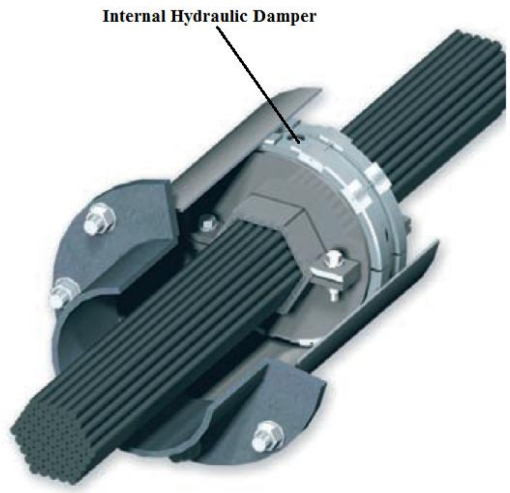

Figure 3.4: Picture of an Internal Hydraulic Damper

The internal hydraulic damper works similar to car shocks in that it uses a viscous fluid to dampen out vibrations. The damper collar has two halves that are wrapped around the cables, the two halves are bolted together and the entire system is held in place by the cable cap that is placed on top of the damper. The damper bladder is filled with a viscous fluid and acts to reduce the vibration of the stays that might be caused by traffic, wind, or other sources (Fressyinet Spec. Sheets).

Below deck level the cables are held in place by a threaded anchor tube that has a collar that matches the cable strand layout for the cable. The bottom of the cable has a drain pipe that allows any moisture that may make it into the tube to exit. Any voids in the bottom of the cable area are filled with wax which acts as a moisture sealing agent. The anchorage system below the deck is enclosed in a galvanized steel cap to protect it from the elements. The anchorage system at the pylon level and deck level are very similar in how the cables are threaded and the anchor system that is used.

The outer sheath that encases the cable strands is a high density polyethylene tube with a double helical fillet exterior rib. The cable sheaths are made in different diameters of 130 (5.12), 150(5.91), 170(6.69), and 190(7.48) mm (in) sizes and the cable lengths vary from 505 feet to 95.2 feet.

3.1.3 Instrumented Cable Locations and Bridge Schematics

To monitor all 152 cables would be financially and practically unfeasible due to the number of sensors, amount of cable, and logistics of monitoring every cable constantly. Therefore, in designing the monitoring system eleven cables were selected to be monitored, nine of the cables are on the east side of the bridge and two are on the west side. Eight are in the same plane and anchor to pylon 6 east; these are expected to provide a good representation of the behavior of the other 3 stay planes. The eleven cables that are being monitored are shown in Table 3.1 (AECOM construction drawings) along with other important information about the cables.

Table 3.1 is organized in succession by where the cables are located on the bridge. For example if traveling from the south to the north the first instrumented cable that would be seen is 219, then 319 and so on. The cables furthest from the pylon at the center line of the main span are the longest and have the highest design tension. Column two, labeled “Length”, is the length L, of the stay from (1.4), the third column, labeled “Linear Mass” is the m, column 4 is the design damping ratio for the cables damper. The length of the cables is taken as the distance from the anchor block below the deck to the anchor point that is inside the pylon as shown in Figures 3.2 and 3.3. The last three columns are design and measured tensions. Column five lists the 10,000 day end of construction tension (the estimate of what the tensions will be in

27+ years), column six the tensions at the end of construction, and the final column are measured cable tensions in December of 2011 (measured by the contractor during final stay tensioning, using a hydraulic jack just before the bridge opened to traffic).

Table 3.1: Details of Instrumented Cables

Cable Locations (1)	Length (ft) (2)	Linear Mass (slug/ft) (3)	Design Damping (%) (4)	Est. Design Tension EOC 10,000 Days (kips) T_{10k} (5)	Est. Design Tension EOC (kips) T_{EOC} (6)	Measured Tension (kips) T_{MH} (7)
219E	505	1.4725	0.59	1517	1438	1439
319E	505	1.4752	0.59	1534	1432	1386
319W	505	1.4752	0.59	1491	1390	1387
315E	407.4	1.0081	0.51	822	768	767
310E	287	0.8852	0.41	836	758	895
310W	287	0.8852	0.41	836	758	872
305E	171.7	0.6147	0.31	608	576	578
404E	154.8	0.5901	0.30	511	491	561
408E	246.6	0.8114	0.37	736	688	725
413E	367.3	0.9343	0.47	970	934	885
419E	458.9	1.4999	0.55	1254	1127	1225

The schematics shown in Figures 3.5 and 3.6 (from construction drawings) are representations of the bridge with the cables labeled and shown. Figure 3.5 shows the south side of the bridge and the cables instrumented on that side and Figure 3.6 shows the north side. Note that the centerline of the mid span is where the two schematics meet.

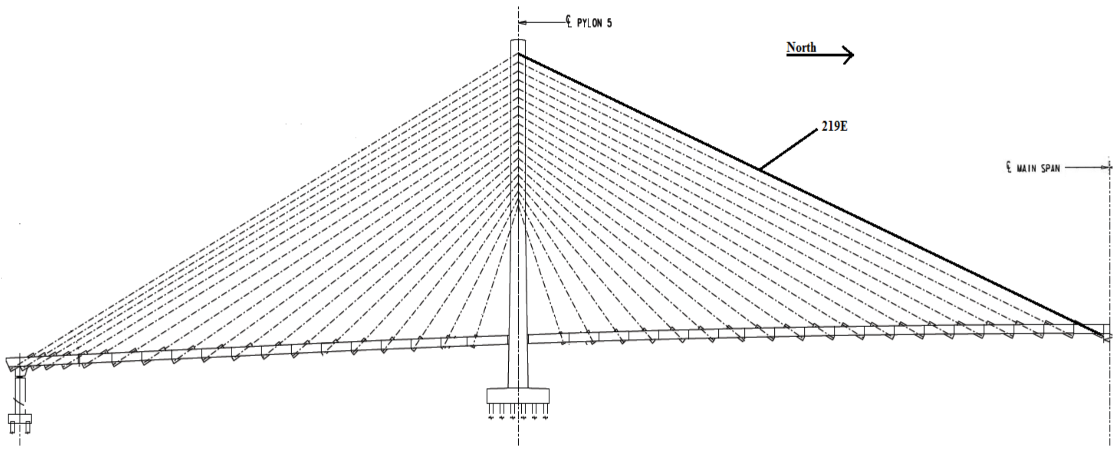

Figure 3.5: Cable Instrumented on the Bridge South Side

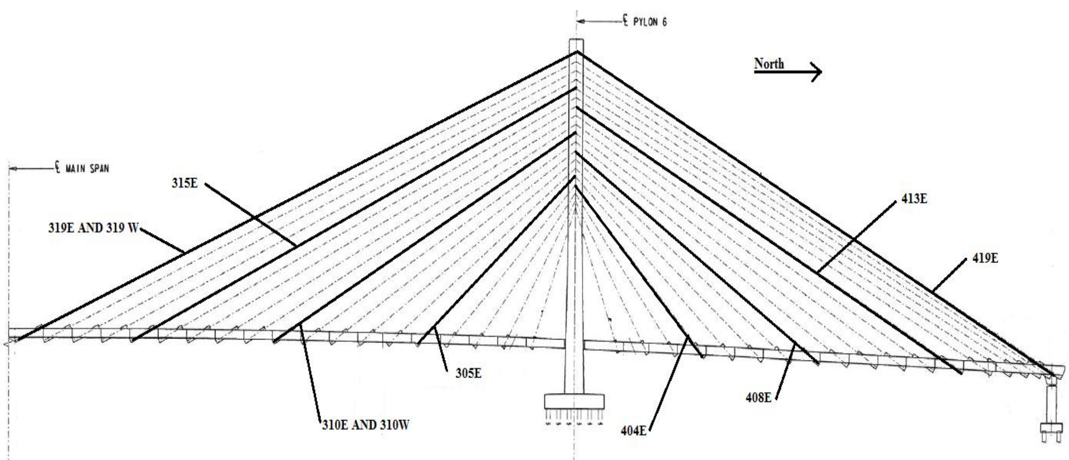

Figure 3.6: Cables Instrumented on the Bridge North Side

3.2 Sensor and Data Acquisition System Descriptions

3.2.1 Sensor Description and Mounting

To measure the vibrations of the cables accelerometers were mounted directly onto the stays. The accelerometers are Micron Optics model OS7100 sensors; one is shown in Figure 3.7. These fiber optic accelerometers are ideal for long term outdoor monitoring due to their metallic casing and armored cable to protect the sensor. The accelerometers can be mounted to measure up to three axes of acceleration. The stand-alone Micron Optics accelerometer is shown in Figure 3.7 (Micron Optics OS7100 technical sheet). Two accelerometers were used on each instrumented stay to measure the vibration of the stay in two orthogonal directions. The mounting fixture for the two is shown in Figure 3.8 (University of Delaware Indian River Bridge Inlet SHM Sensor Detail Sheet, Detail E).

Figure 3.7: Single Axis Micro Optics Accelerometer

The two sensor mount shown in

Figure 3.8 was designed to measure cable accelerations in the Y and Z directions. The accelerometers are mounted to a plate that is clamped around the diameter of the cable at approximately 35 feet above the deck. The plates are mounted on the outside of the bridge meaning that they do not face traffic and are not visible from the pedestrian walkway or the travel lanes. The plate is mounted parallel to the direction and inclination angle of the cable.

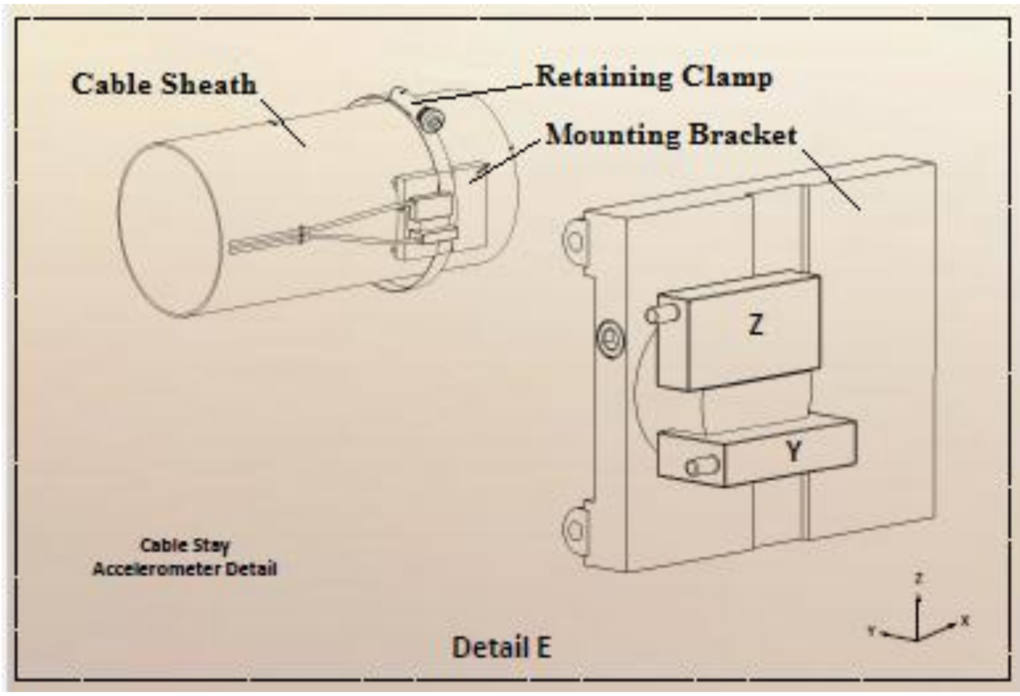

Figure 3.8: Two Accelerometer Mounting Schematic

The sensor layout below in Figure 3.9 better describes how the sensors are mounted on the cable.

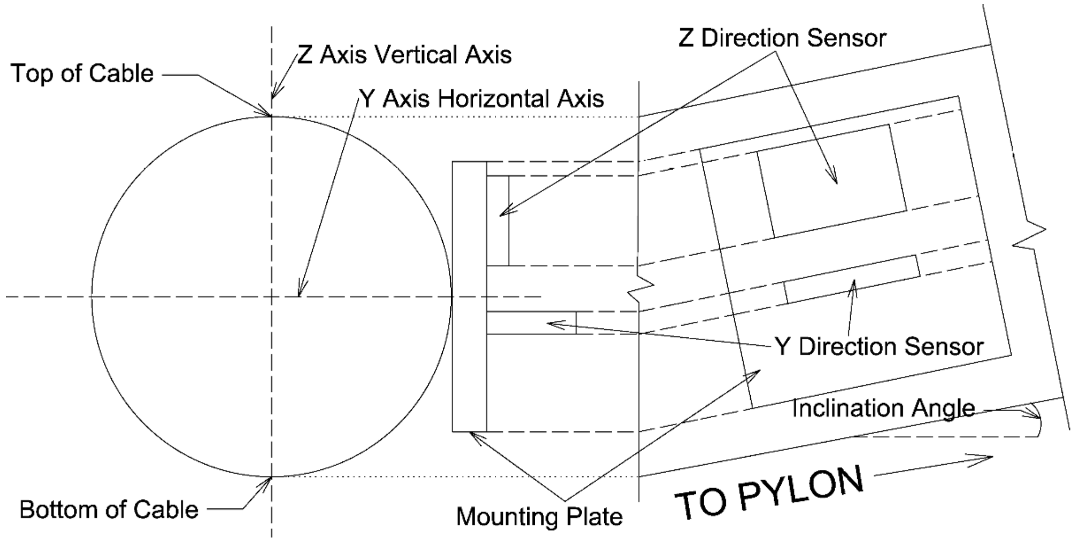

Figure 3.9: Cable Mounting Orientation

Figure 3.8 shows that the sensors are mounted to measure horizontal and vertical vibrations in the cables. The right hand side of Figure 3.9 shows how the cables mounting bracket is oriented on an inclined cable. The Z direction sensors measure vibrations in the plane of the stays (positive Z is perpendicular to the stay and in the plane of the stays, positive measuring up) and the Y direction sensors measure vibrations transverse to the plane of the stays (positive Y is perpendicular to the plane of the stays and toward the east).

The accelerometers have a frequency range of up to 300 Hz and a mounted resonance frequency of approximately 700 Hz. However, the manufacturer reports that each sensor has a unique mounted resonance frequency characteristic to that sensor. The maximum frequency range of the sensor far exceeds the frequency requirements needed to measure the predominate frequencies of the stay cables, which using the data in Table 3.1 and (1.4) are found to be well below 50 Hz. The resonant frequency is important in avoiding aliasing of the signal: this phenomenon will be discussed in more detail in later sections.

3.2.2 Data Acquisition System

The data acquisition system is designed for long term structural health monitoring of any structure. The system can monitor many different types of fiber based sensors. The data acquisition system that is being used is a Micron Optics interrogator model SM130 sensing module shown in Figure 3.10 (Micron Optics SM130 Technical Sheet). The module is designed to respond to user commands from an external computer that is linked to the module by an Ethernet cable.

Figure 3.10: Micron Optics Interrogator

The SM130 is also designed so that custom computer software can be used to control the sensing module with any of a wide range of user interface software and platforms. The system is also useful because it can be synchronized with multiple interrogators. Also, the module is capable of sampling at a wide range of frequencies and at a wide range of wavelengths which is optimal for putting multiple sensors on one channel. The SM130 can sample at rates up to 1 kHz and has a wavelength range from 1510-1590 nm (Tech. Sheet SM130). This module is practically equipped for the long term objectives of this project as it has flexible scan rates and capabilities to obtain large data sets.

3.3 Computer and Analysis Methods

The data from the data acquisition system is recorded as a time history of acceleration versus time. The time history data can be explicitly analyzed to estimate the frequencies of the stays, but this requires counting of peaks and calculating periods of the cables. The data acquisition system and computer methods make the process of extracting natural frequencies much more automated and reduce the amount of time needed to calculate natural frequencies. Also, using certain computer methods allows for more than one natural frequency to be estimated from a data set.

3.3.1 Period Counts

One way of estimating the natural frequency from a time history is to count peaks and find the natural period of the cable. The natural period is the inverse of the natural frequency ($f = 1/T$), so finding the natural period is an easy, fast way to find the natural frequency. The natural period is the time it takes to complete one full oscillation and can be found easily from acceleration data, if there is a clear single frequency component in the signal. If there is not a dominant frequency this becomes much more difficult. Shown in Figure 3.11 is an example of a theoretical free vibration response of a single-degree-of-freedom system and the natural period calculated from the data.

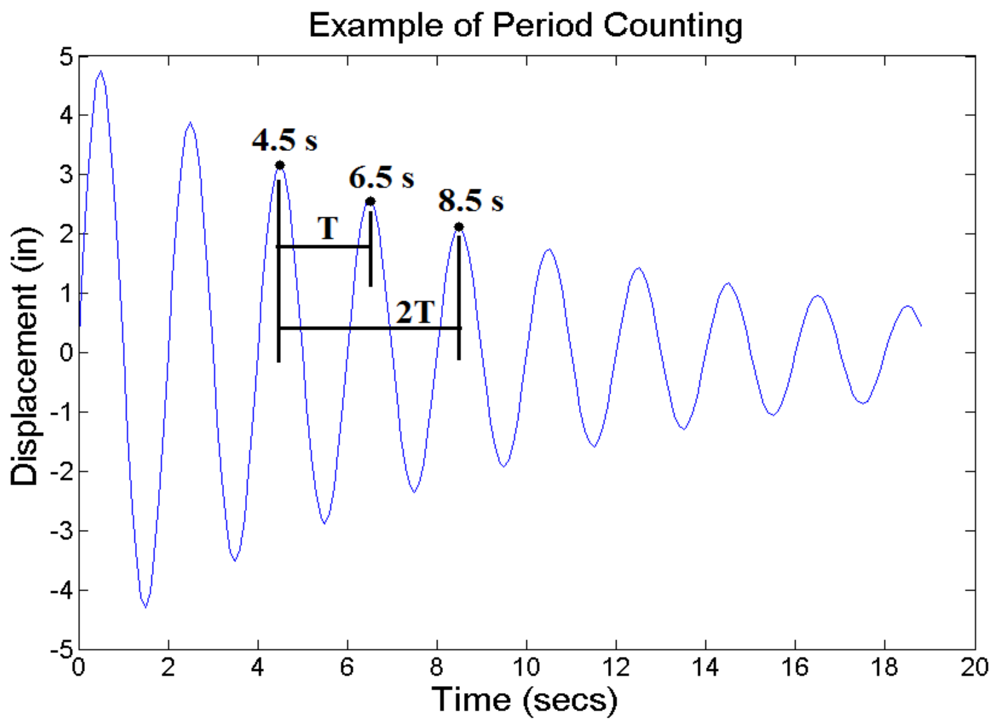

Figure 3.11: Example of Period Counting

The three times 4.5, 6.5, and 8.5 sec represent period peaks in the data. Period counting is just the difference in the time of the peaks divided by the number of peaks between the two times. For example, (6.5-4.5)/1 would give a fundamental period of 2.0 seconds. To calculate the period between multiple peaks you simply divide by the number of peaks, e.g., (8.5-4.5)/2 yields the same answer of 2.0 seconds. This example is a very simple theoretical result that yields the same natural period for any number of peaks which translates to the same natural frequency of 0.50 Hz. Using actual ambient vibration acceleration data the peaks aren't always spaced perfectly and the fundamental period is not always exactly the same, thus the peak difference approach is not well suited for estimating the stay frequencies.

3.3.2 Fourier Transforms

Finding multiple embedded frequencies in time history data can be very difficult. Instead of explicitly analyzing data using period counting, using the power spectra of a signal is a much easier way to analyze large data sets. To get frequencies from time history data it must be transformed into the frequency domain, using the properties of the power spectral density it is possible to change domains. The power spectral density shows the distribution of a signal or time history over a range of frequencies. Unlike transient pulse like signals that can be described by simple Fourier transforms, the power spectral density is useful in defining continuous signals and time histories. These continuously "infinite" signals fall into a category of stationary random processes, characterized by the joint probability distribution remaining unchanged regardless of where the statistics are taken in the time history. Assuming that the collected data is a stationary, defining the time histories power spectral density is appropriate because it defines the power of the signal over a range of frequencies. This translates simply to the natural frequencies of a cable where the higher the power of that frequency in the time history the more dominant that frequency is to the entire cables vibration. An example of a power spectral density is shown below in Figure 3.12.

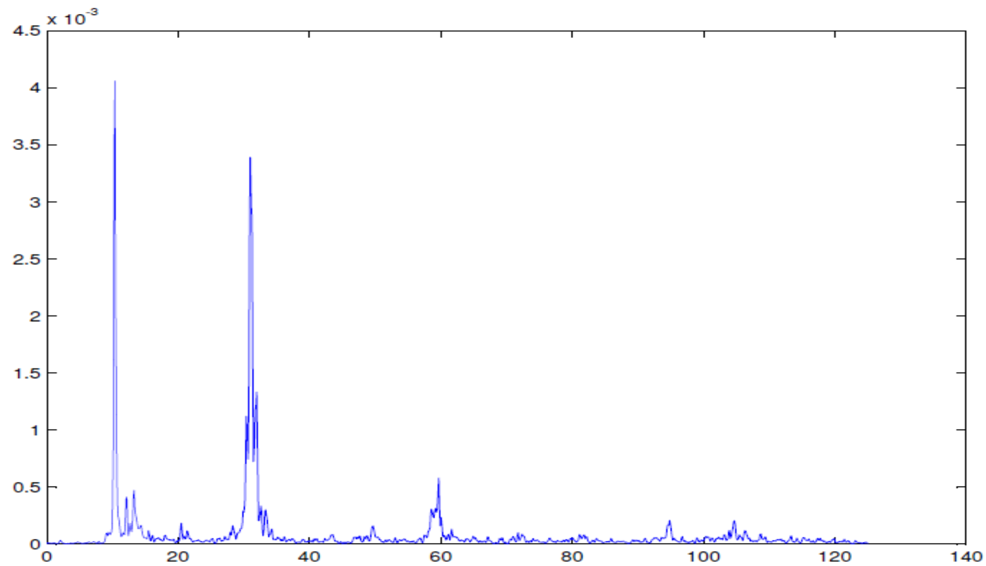

Figure 3.12: Example of Power Spectral Density MATLAB Output

The example shown in Figure 3.12 is the power spectral density output from a test conducted in the laboratory on a 20 foot thin wire which was excited at various places along its length. The time history was recorded using analog accelerometers and then processed through a MATLAB program to find the power spectral density. The spectra shows the dominant frequencies of the cable are at 10, 30, and 60 Hz.

3.3.3 Computer Methods

To get more accurate estimates for each accelerometer large data files need to be used; therefore the data files get very large, with upwards of 70,000 data points. Processing that much data individually would be extremely time-consuming. Instead of processing and analyzing each individual accelerometer, simultaneously extracting, processing, and analyzing acceleration data can be done using various MATLAB commands. A MATLAB script file was developed to automate the processing of the acceleration data files. The MATLAB script file is found in Appendix B. To calculate the power spectral density the MATLAB command “cpsd” was applied to the data set.

The command computes the cross-spectral density of the input time histories; when a signal is crossed against itself the power spectra density is produced. The command uses a Welch averaging periodogram to estimate the spectral density of the given acceleration data. After that data is processed it can be plotted to get results that will have similar characteristics as Figure 3.11, in that there will be well defined peaks that are fundamental frequencies.

Chapter 4

PLUCKED VIBRATION DATA AND ANALYSIS

4.1 Pluck Test

In a pluck test the stay is set into motion and then released and allowed to vibrate freely. In a simple laboratory test a cable can be “plucked” just like a guitar string. However, on the Indian River Inlet Bridge the stays are too large to pluck in that manner; therefore, direct manpower is used to shake the stay, set it into motion, and then it is released and allowed to vibrate freely. To conduct the test a bucket truck was used to lift a person up away from the anchorage point and damper at the cable base to avoid the vibrations being damped out to quickly. The cables were first shaken in the Y direction and the motion recorded, then shaken in the Z direction and the motion recorded. Two pluck tests were performed, the first on May 11th 2012 in which all the cables on the east side except for 419E were tested. The second occurred on May 5th 2013 as part of the one year load test for the bridge in which cables 219E, 319E, 319W, and 413E were tested.

Using columns (5), (6), and (7) in Table 3.1 with equation (1.4) the natural frequencies of the stays can be estimated for certain loading types. In Table 4.1 the first six natural frequencies (denoted as f_{EOC}) are shown using the estimated design tensions from the end of construction column (6). The table shows the trend that the shorter the cable the higher the first natural frequency will be. For example, cable 404E, which happens to be the shortest cable in the set, has the highest first natural frequency. The longer cables have smaller frequencies translating to longer periods which follow convention. 419E has the smallest frequency; although it is the same length as 319E and 219E other parameters affect the frequency as seen in equation (1.3).

Table 4.1: Estimated Natural Frequencies from EOC Design Tensions (f_{EOC})

	Estimated Natural Frequency (Hz)					
	Mode Number					
Cable	n=1	n=2	n=3	n=4	n=5	n=6
219E	0.9775	1.9555	2.9325	3.9100	4.8875	5.8651
319E	0.9754	1.9509	2.9264	3.9018	4.8777	5.8528
319W	0.9611	1.9221	2.8832	3.8442	4.8053	5.7663
315E	1.0712	2.1425	3.2136	4.2848	5.3561	6.4273
310E	1.6121	3.2243	4.8365	6.4487	8.0608	9.6730
310W	1.6111	3.2222	4.8333	6.4444	8.0555	9.6666
305E	2.8189	5.6378	8.4567	11.2755	14.0945	16.9134
404E	2.9462	5.8925	8.8388	11.7851	14.7314	17.6776
408E	1.8670	3.7340	5.6011	7.4681	9.3352	11.2022
413E	1.3610	2.7220	4.0831	5.4441	6.8051	8.1662
419E	0.9444	1.8889	2.833	3.7778	4.7223	5.6668

In Table 4.2 are the frequencies obtained when using the tensions listed in column (7) of Table 3.1, which are the stay tensions measured by the contractor at the end of construction, using a hydraulic jack. These are denoted as $f_{MH.}$ The reason for having these estimated frequencies is to have a comparison point between the design tensions, hydraulically measured tensions, and tensions measured from the acceleration data.

Table 4.2: Estimated Frequencies from Hydraulic Jack Tensions (f_{MH})

Estimated Natural Frequencies (Hz)						
	Mode Number					
Cable	n=1	n=2	n=3	n=4	n=5	n=6
219E	0.9778	1.9557	2.9335	3.9114	4.8892	5.8671
319E	0.9597	1.9193	2.8790	3.8386	4.7984	5.7580
319W	0.9600	1.9200	2.8801	3.8401	4.8000	5.7601
315E	1.0705	2.1410	3.2115	4.2821	5.3526	6.4231
310E	1.7518	3.5036	5.2554	7.0072	8.7590	10.5108
310W	1.7291	3.4583	5.1875	6.9166	8.6457	10.3749
305E	2.8238	5.6476	8.4714	11.2951	14.1189	16.9428
404E	3.1492	6.2986	9.4479	12.5971	15.7564	18.8958
408E	1.9166	3.8332	5.7497	7.6663	9.5829	11.4994
413E	1.4204	2.8407	4.2611	5.6815	7.1018	8.5222
419E	0.9847	1.9694	2.9540	3.9387	4.9233	5.9081

The first pluck test frequency results are displayed in Table 4.3. It is important to note that only eight of the eleven cables were able to be tested due to accessibility issues with sensors 319W and 310W and sensor 419E was not operational at the time. The table displays three main columns, Y and Z direction results and an averages column. The major Y and Z column headings are the direction in which the cable was shaken, which follows the directional orientation described in Figure 3.9. The sub heading under the major headings is the frequency at which an obvious distinct peak occurred. The table does not take into account mode numbers but is simply a record of what frequencies were identified from the spectra. An “-” indicates that a clear second or third peak could not be discerned in the spectra for that sensor.

In theory, since the stays are circular and basically uniform in cross-section, the frequencies in the Y and Z directions should be approximately equal, i.e., the peaks in the Y direction column and the Z direction column should be the same; therefore, the average of the peaks was calculated and is reported in the final “Average” column. In general when comparing the peaks of both sensors they tend to have small variations.

Table 4.3: Measured Frequencies (Hz) from May Pluck Test (f_{MF})

	Y Direction			Z Direction			Average		
Cable	1^{st} Peak	2^{nd} Peak	3^{rd} Peak	1^{st} Peak	2^{nd} Peak	3^{rd} Peak	1^{st}	2^{nd}	3^{rd}
219E	1.892	3.784	5.676	1.892	3.784	-	1.892	3.784	5.676
319E	1.831	3.693	-	1.831	3.708	-	1.831	3.701	-
315E	2.136	4.211	-	2.136	4.211	6.348	2.136	4.211	6.348
310E	1.709	3.418	-	1.709	3.4188	5.188	1.709	3.418	5.188
305E	2.686	5.401	-	2.686	5.371	-	2.686	5.386	-
404E	2.93	-	-	2.93	-	-	2.93	-	-
408E	1.77	3.601	5.402	1.77	3.601	-	1.77	3.601	5.402
413E	1.221	2.441	-	1.221	2.502	3.784	1.221	2.472	3.784

Figure 4.1 is an example of time history data used to get the cpsd shown in Figure 4.2. This shows a significant amount of overlap in the two sensors which explains why the results are similar and produce like frequencies.

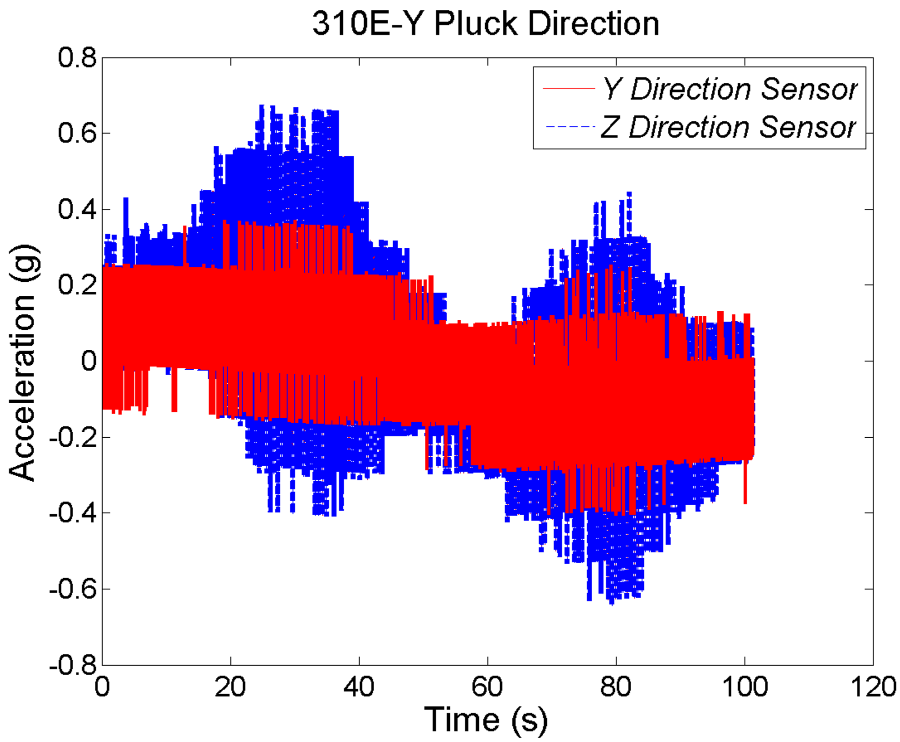

Figure 4.1: Time History of Cable 310E from May Pluck Test

Figure 4.2 is an example spectra for data that has two distinct frequency spikes but has no third peak in the data sample.

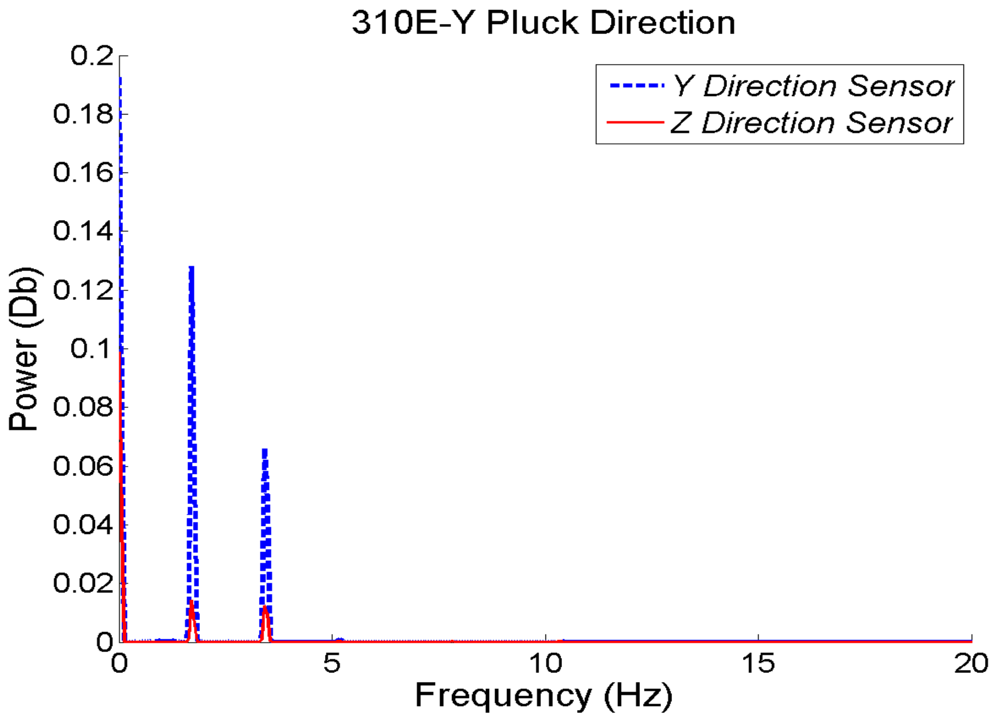

Figure 4.2: Example of CPSD from Plucked Vibration Data

Figure 4.2 shows the spectra for cable 310E shaken in the Y direction (the letter in the title of the graph after the hyphen indicates the direction the cable was shaken). Note that both sensors were plotted on the same graph to visually show any overlap that may occur. In Figure 4.2 there is a significant amount of overlap in the signals even though the power of the Z oriented sensors power is significantly lower. For each data sample only the peaks from the sensors oriented in the same direction as the cable was shaken were recorded, for example, only the Y-direction sensor data was recorded in Figure 4.2. The first and second frequency peaks recorded were 1.709 Hz and 3.418 Hz respectively and no third frequency peak was recorded as there was no significant frequency available to be recorded. Figure 4.3 is an example of the data used to find the cpsd in Figure 4.4.

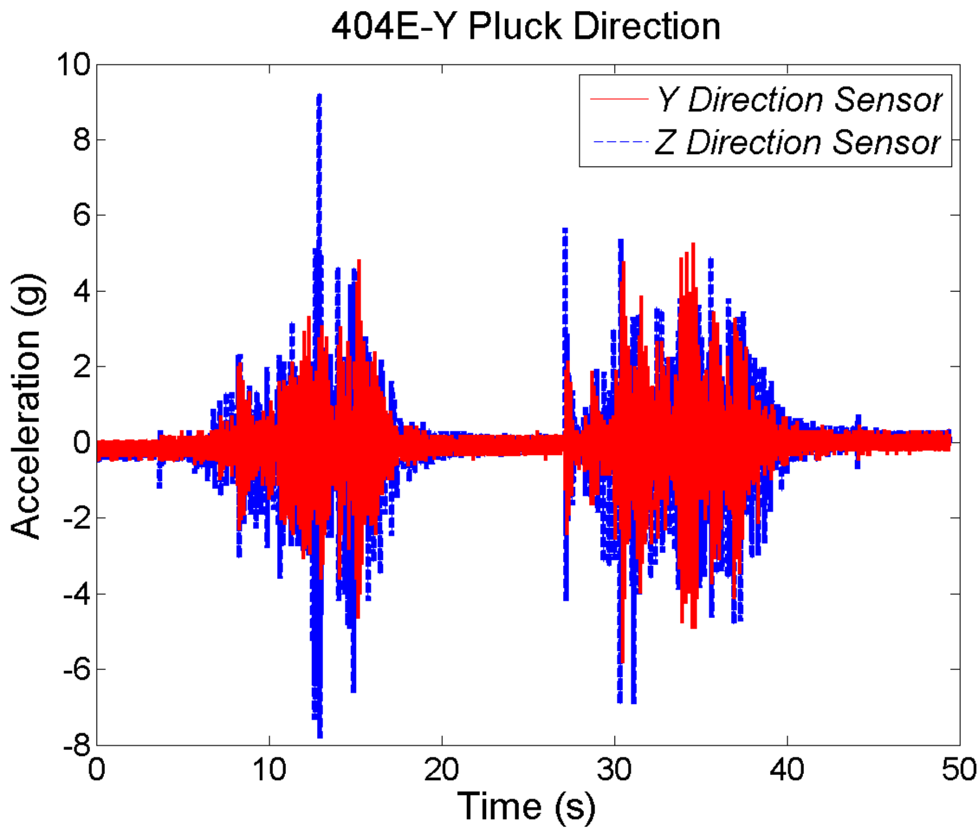

Figure 4.3: Time History for Cable 404E from May Pluck Test

Like in Figure 4.1, 4.3 display a significant amount of overlap in both the Y and Z accelerometers. Figure 4.4 is the CPSD of the accelerometer data from Figure 3.3.

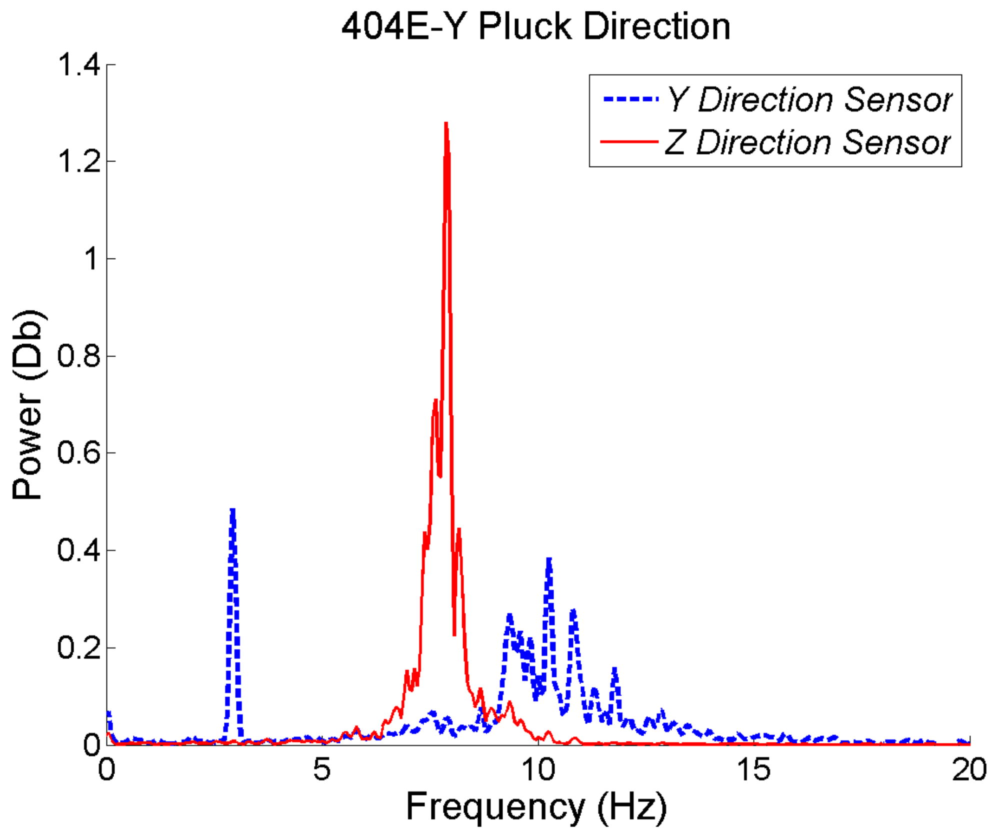

Figure 4.4: Example of CPSD Data with Signal Washout

Unlike Figure 4.1, which shows two well defined frequency spikes then tails off to show no other significant peaks, Figure 4.4 is an example of a spectra that shows a wide band of significant power in the range of frequencies of interest. This wide bank "noise" was present in a number of spectra and made identifying distinct frequencies difficult. Although one well defined peak is seen at 2.93 Hz, the signal becomes choppy with multiple peaks packed into a small frequency range making it impossible to determine which frequency spike can be used. The frequency spike between 5 and 10 Hz is an example of a signal affected by aliasing, which will be discussed in detail in Chapter 5. The remaining CPSD plots for the frequency data shown in Table 3.1 are shown in Appendix A.

In the second pluck test (May 5, 2013) the first plucked vibration data for 319W is seen as well as comparison data 219E, 319E, and 413E. The data gathered from 319W shows the presence of aliasing in most if not all the test data as seen in Figure 4.5 and 4.6. Figure 4.5 shows when the cable was shaken in the Y direction, Figure 4.6 shows the cable being shaken in the Z direction.

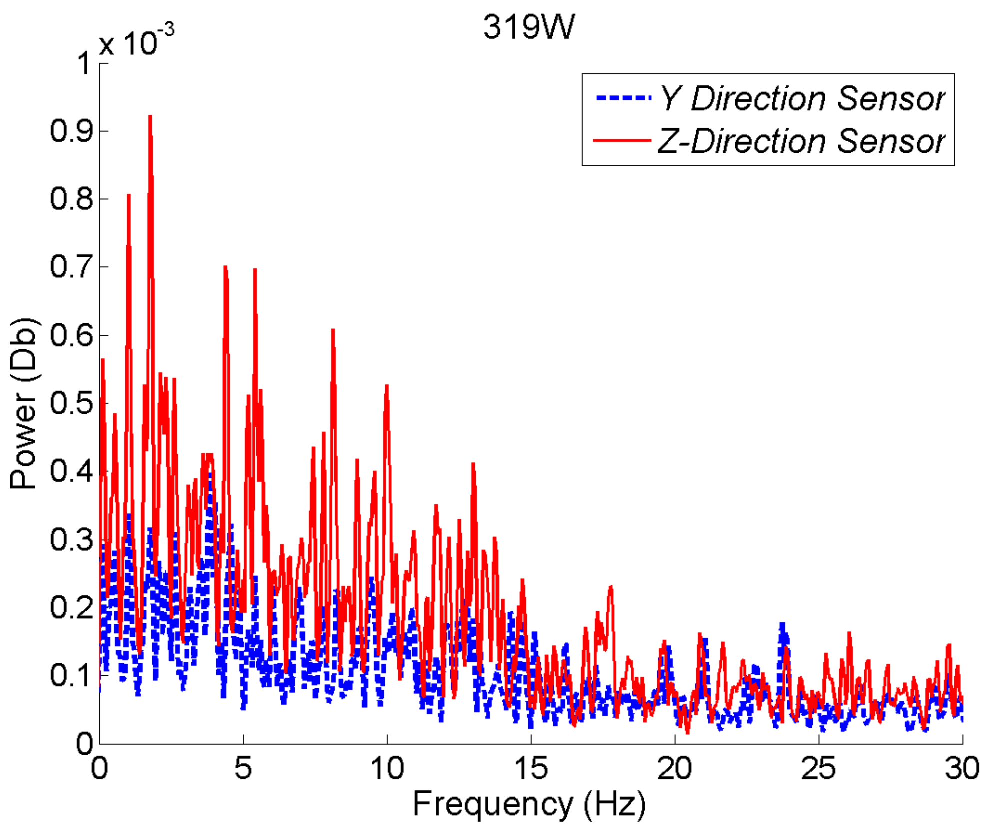

Figure 4.5: 319W Pluck Test CPSD Shaken in the Y-Direction

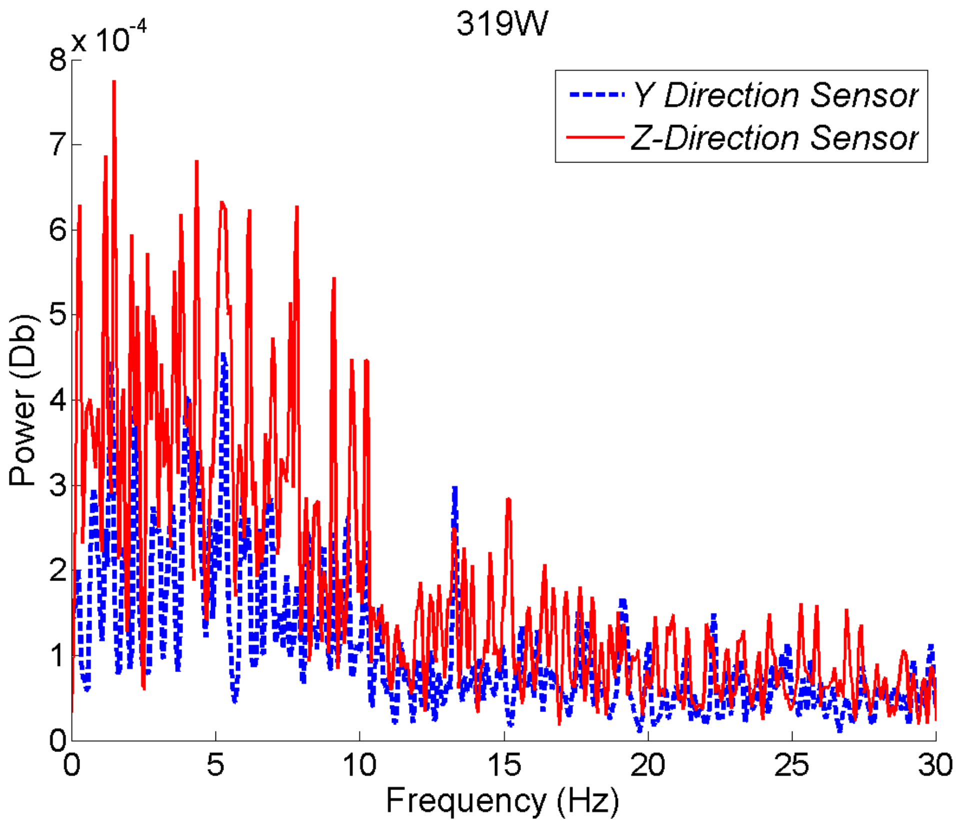

Figure 4.6: 319W Pluck Test CPSD Shaken in the Z-Direction

From these two figures nothing can really be deciphered. Any frequency that would be pulled from these two data sets would be purely based on previous knowledge of the estimated fundamental frequencies. There are no discernible frequency peaks that can be used with any accuracy or confidence that the peak is the actual frequency at which the cable is vibrating.

319E did not have the considerable amount of aliasing seen in 319W but produced undesirable results with no obvious peaks. Figure 4.7 and 4.8 are examples of 319E shaken in the Y direction and Z direction respectively.

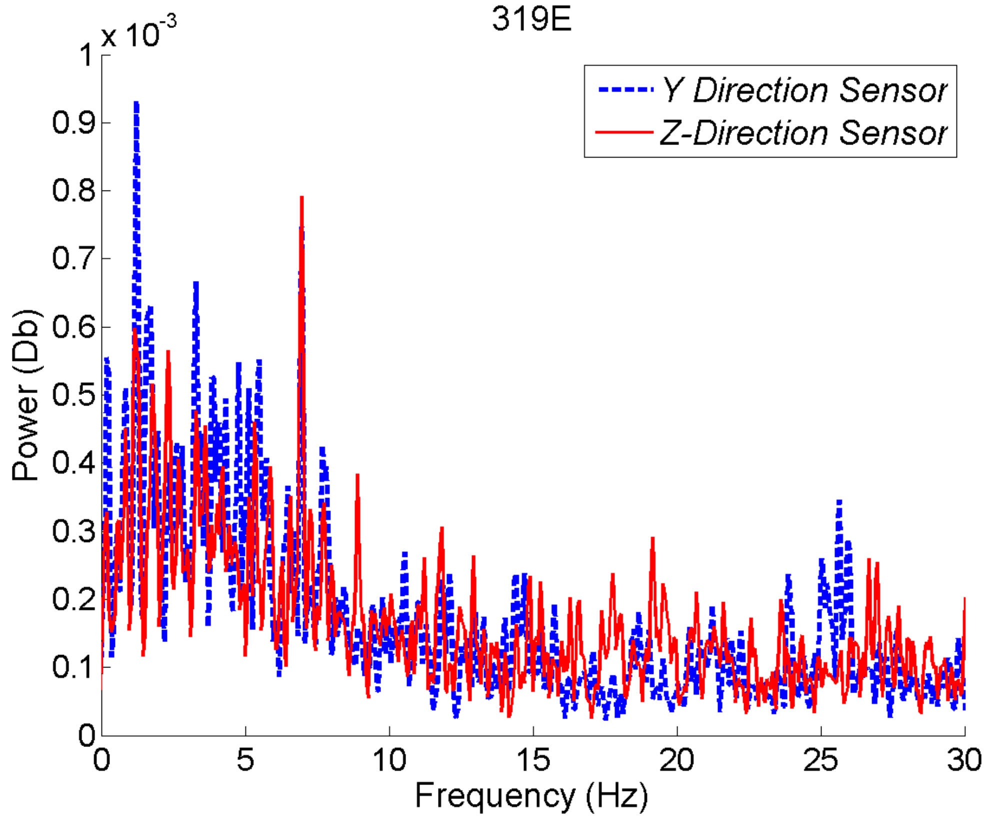

Figure 4.7: 319E Pluck Test CPSD Shaken in the Y-Direction

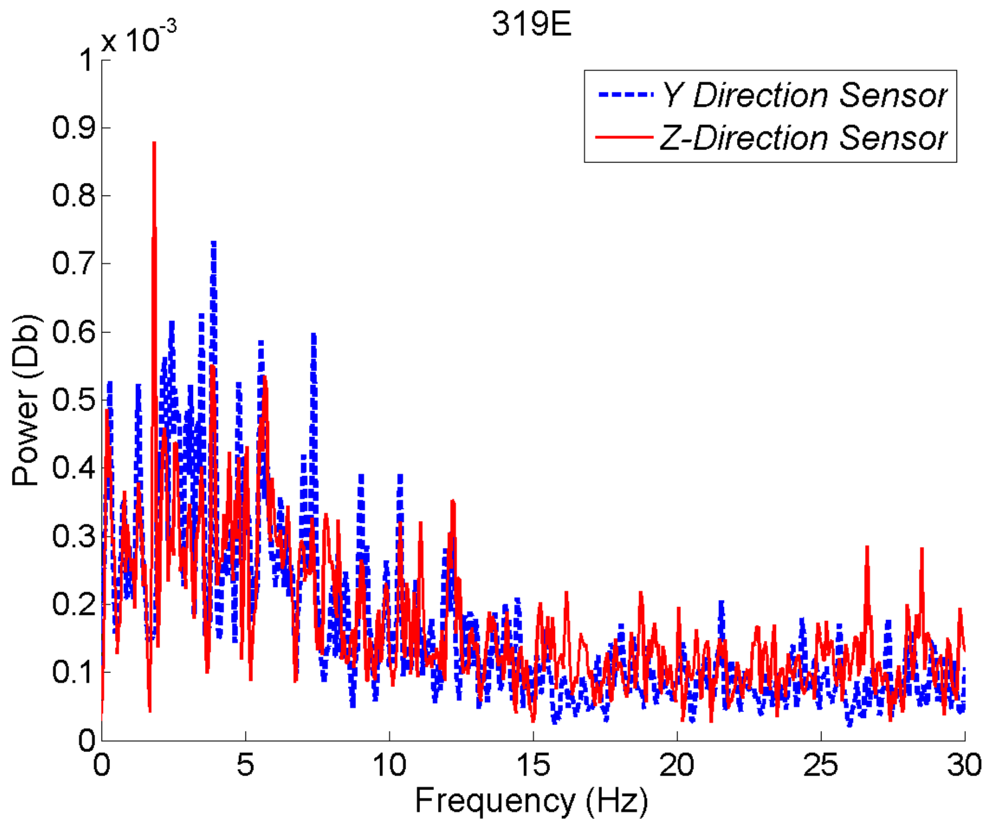

Figure 4.8: 319E Pluck Test CPSD Shaken in the Z-Direction

Like in the 319W results the aliasing is seen in the first 15 Hz of the CPSD signal. No frequencies from these data can be used for tension estimations.

The cable data from 219E produced obvious frequency peaks that can be used for tension estimation. Figure 4.9 and 4.10 show the CPSD data for 219E shaken in the Y direction and Z direction respectively.

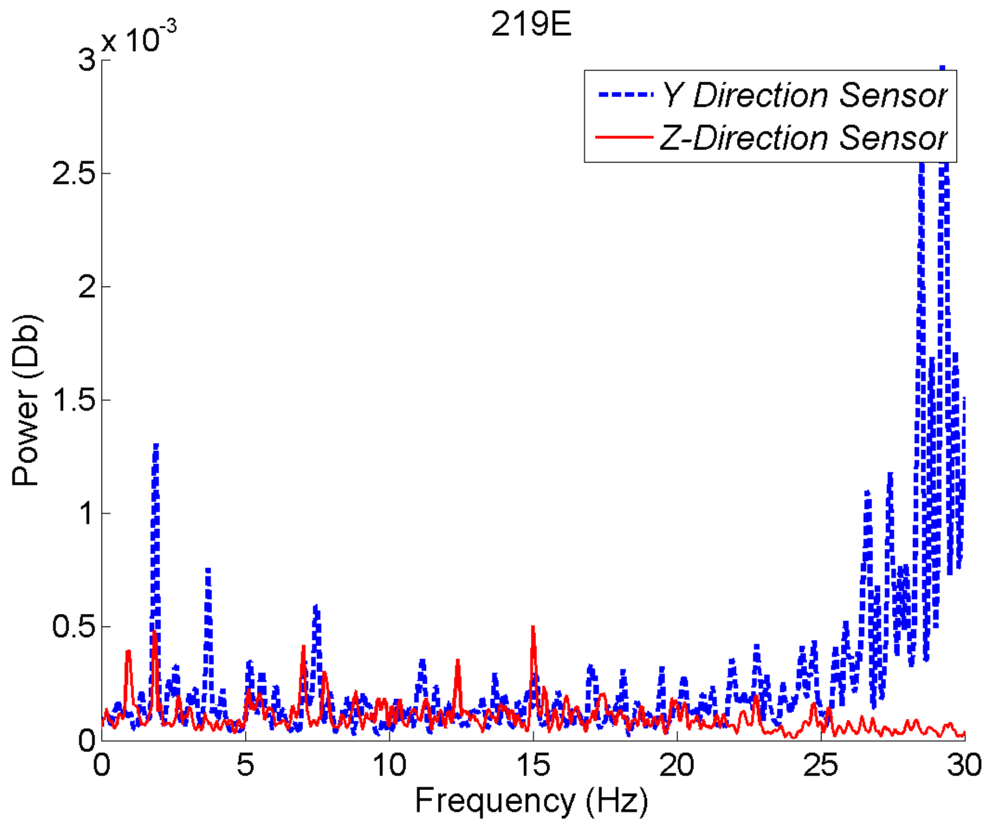

Figure 4.9: 219E Pluck Test CPSD Shaken in the Y-Direction

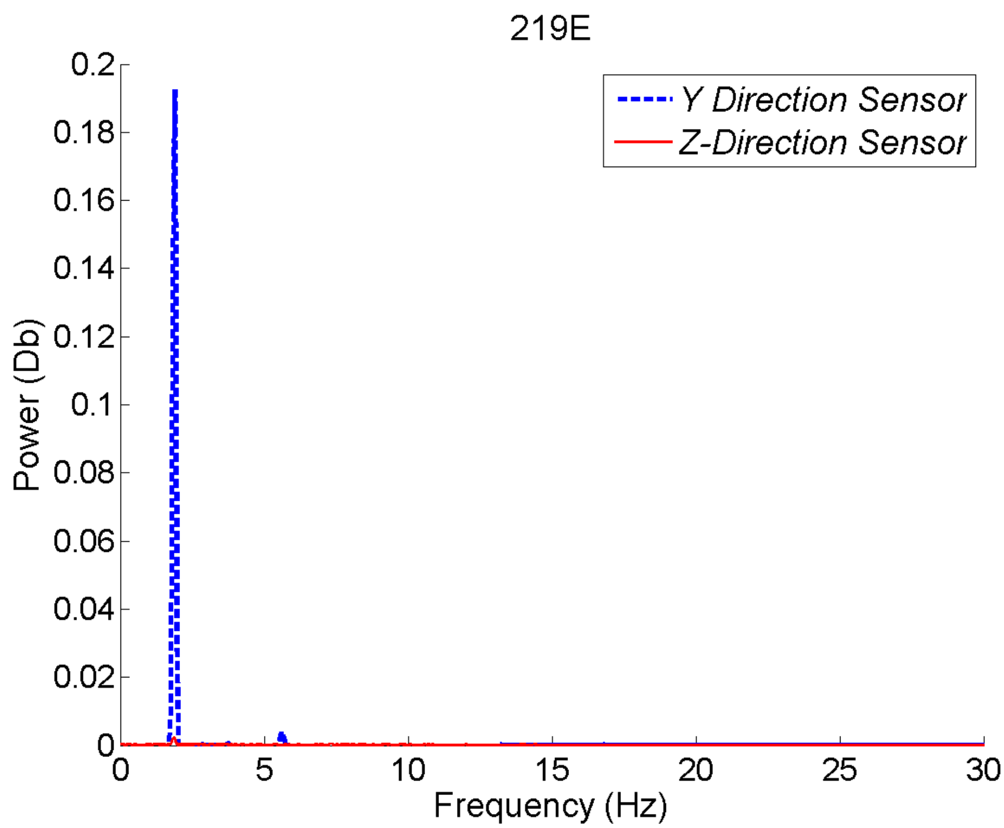

Figure 4.10: 219E Pluck Test CPSD Shaken in the Z-Direction

Note that the peaks in for both figures are easily found in comparison to the rest of the signal. In Figure 4.11 and 4.12 the CPSD graph for 413E is shown shaken in the Y direction and Z direction respectively.

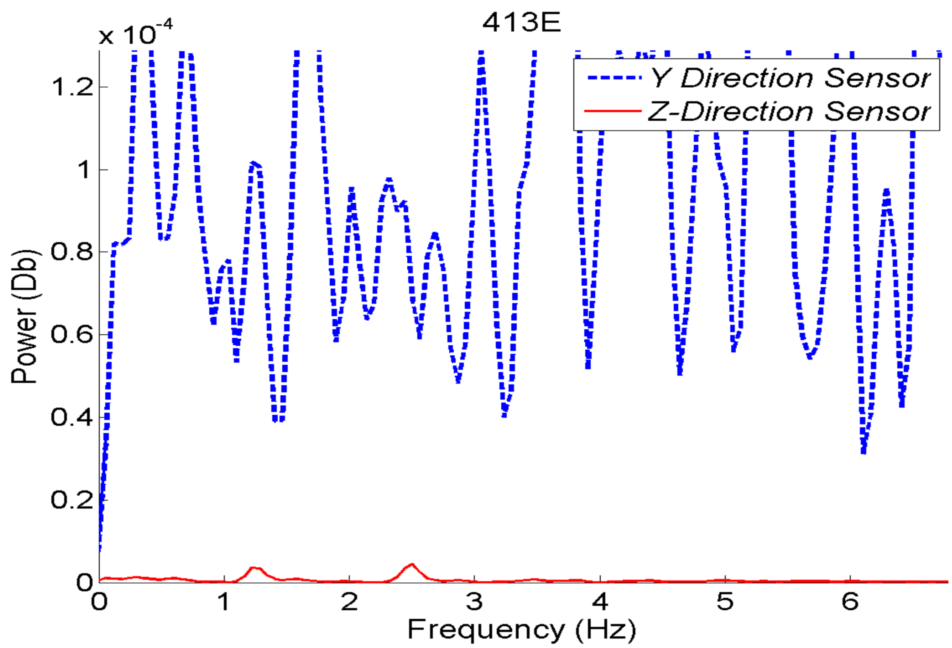

Figure 4.11: 413E Pluck Test CPSD Shaken in the Y-Direction

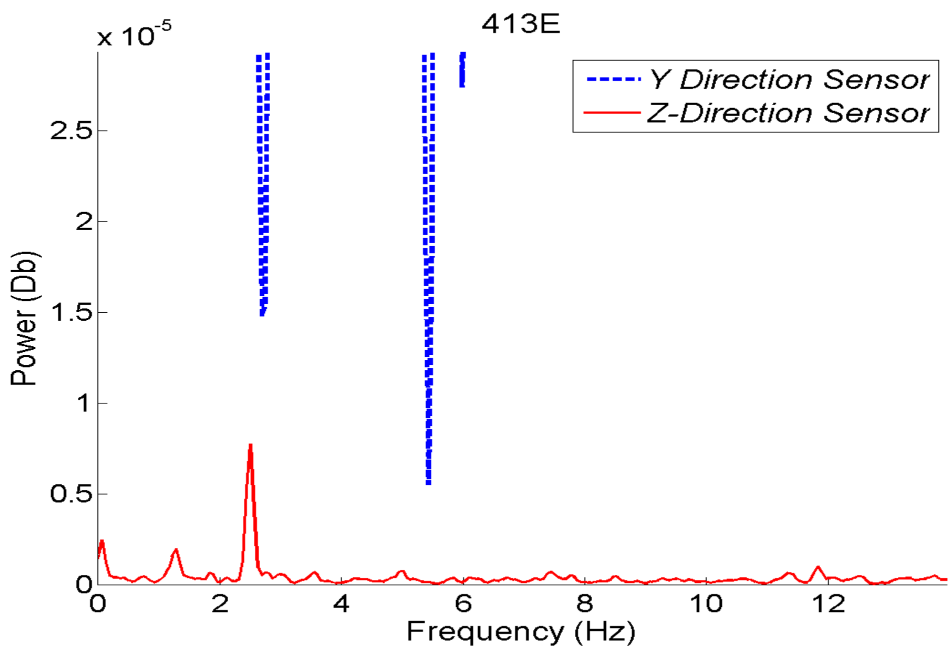

Figure 4.12: 413E Pluck Test CPSD Shaken in the Z-Direction

In the figures for 413E only the first few Hz of the graph is shown. This is because the power of the peaks was very small in the Z direction and needed to be zoomed in on. The data is not altered when doing this only the display of data is altered. The Y direction sensor in Figure 4.11 and 4.12 is not useful as there are not obvious peaks and it looks like the data presented for 319E. Although the peaks in 413E are small they are still associated with a frequency of vibration and are clearly peaks compared to the data around them.

4.2 Pluck Test Analysis

Comparing the frequency results from the pluck test to the frequencies in Tables 4.1 and 4.2, the frequencies for the most part are similar; however, a noticeable difference does occur in the first three cables listed in the tables. For these, the measured frequencies from the pluck test in rows 1-3 ($\bar{f}$) are almost double the frequencies seen in Table 4.1 (f_{EOC}). A simple explanation for this is that the accelerometers are simply not picking up the odd modes of vibration (n =1,3,5, etc…) because the stay was not shaken in a manner that would excite an odd mode.

In conducting the pluck test the hope was that the stay would be excited in the first mode of vibration. However, if a stay was excited predominately in a higher mode, for example the second mode, the higher frequency would be most prevalent in the spectra and the fundamental frequency may not appear in the spectra. This was most likely to happen for the longer stays where it was not possible to reach the mid-point of the stay where it would be easiest to excite a first mode response.

A quick calculation using (1.4) and those frequencies ($\bar{f}$) show that the tensions are close to three times larger than the estimated tensions from the hydraulic test and end of construction loads from Table 3.1. Re-mapping the average frequencies in accordance to which mode of vibration they are assumed to be yields Table 4.4. Note that any cable designator with an * is data from the May 2013 test.

Table 4.4: Average Frequencies Mapped with Mode Number ($\bar{f}$)

Estimated Frequencies (Hz)						
	Mode Number					
Cable	n=1	n=2	n=3	n=4	n=5	n=6
219E	-	1.892	-	3.784	-	5.676
219E*	-	1.877	-	3.723	-	5.615
319E	-	1.831	-	3.701	-	-
315E	-	2.136	-	4.211	-	6.348
310E	1.709	3.418	5.188	-	-	-
305E	2.686	5.386	-	-	-	-
404E	2.93	-	-	-	-	-
408E	1.77	3.601	5.402	-	-	-
413E	1.221	2.472	3.784	-	-	-
413E*	1.241	2.502	-	-	-	-

*Frequencies from plucked data from May 5th 2013 test

The frequencies and mode numbers in Table 4.4 are used to calculate the tension from measured vibrations. This is the first step in accomplishing the objective of this research in estimating tensions from measured natural frequencies. Below in Table 4.5 are the estimated tensions that are calculated from the frequencies in Table

4.4, using equation (1.4) with the appropriate parameters found in Table 3.1. These tensions will be used in further sections for comparison to other sets of tensions.

Table 4.5: Estimated Tensions ($\overline{T}$) from Measured Natural Frequencies

	Estimated Tensions(kips) from Pluck Test Data						
	Mode Number						
Cable	n=1	n=2	n=3	n=4	n=5	n=6	Average
219E	-	1346.79	-	1346.79	-	1346.79	1347
219E*	-	1325.17	-	1303.72	-	1318.00	1316
319E	-	1261.35	-	1288.36	-	-	1275
315E	-	763.40	-	741.75	-	749.17	751
310E	851.79	851.79	872.18	-	-	-	859
305E	522.97	525.70	-	-	-	-	524
404E	485.59	-	-	-	-	-	486
408E	618.34	639.84	639.96	-	-	-	633
413E	751.69	770.27	802.17	-	-	-	775
413E*	776.94	789.10	-	-	-	-	783

*Denotes tensions from plucked data from May 5th 2013 test

4.2.1 Frequency Comparison

Before comparing tensions the estimated and measured frequencies will be compared first. Table 4.6 shows the ratio of the measured frequencies from Table 4.4 to the end of construction tension frequencies from Table 4.1, i.e. $\overline{f}/f_{EOC}$

Table 4.6: Comparison of Frequencies from Plucked Data Frequencies and End of Construction Tensions ($\bar{f}/f_{EOC}$)

	Frequency Ratio ($\bar{f}/f_{EOC}$)					
	Mode Number					
Cable	n=1	n=2	n=3	n=4	n=5	n=6
219E	-	0.9678	-	0.9678	-	0.9678
219E*	-	0.9601	-	0.9522	-	0.9573
319E	-	0.9385	-	0.9485	-	-
315E	-	0.9970	-	0.9828	-	0.9877
310E	1.0601	1.0600	1.0727	-	-	-
305E	0.9529	0.9553	-	-	-	-
404E	0.9945	-	-	-	-	-
408E	0.9480	0.9644	0.9646	-	-	-
413E	0.8971	0.9081	0.9267	-	-	-
413E*	0.9118	0.9192	-	-	-	-

*Comparison of May 5th 2013 pluck test frequencies

The results presented in Table 4.6 show that the frequencies that were measured during the pluck test are very similar to the frequencies calculated using the end of construction tension. The ratios range from 0.90 to 1.06, indicating that the sensors are picking up frequencies corresponding to estimated design tensions. The frequencies comparison of column (7) in Table 3.1 is shown in Table 4.7, i.e. $\bar{f}/f_{MH}$.

Table 4.7: Comparison of Frequencies from Plucked Data Frequencies and Measured Hydraulic Tensions ($\bar{f}/f_{MH}$)

	Frequency Ratio ($\bar{f}/f_{MH}$)					
	Mode Number					
Cable	n=1	n=2	n=3	n=4	n=5	n=6
219E	-	0.9674	-	0.9674	-	0.9674
219E*	-	0.9598	-	0.9518	-	0.9574
319E	-	0.9540	-	0.9641	-	-
315E	-	0.9977	-	0.9834	-	0.9883
310E	0.9756	0.9756	0.9872	-	-	-
305E	0.9487	0.9512	-	-	-	-
404E	0.9304	-	-	-	-	-
408E	0.9235	0.9394	0.9395	-	-	-
413E	0.8596	0.8702	0.8880	-	-	-
413E*	0.8744	0.8808	-	-	-	-

*Comparison of May 5th 2013 pluck test frequencies

The results shown in Table 4.7 show that the measured frequencies from the hydraulic test are almost the same, in some cases closer, to the measured frequencies from the plucked test data. The range of the data is between 0.92 and 0.99 indicating that tensions from the cables are lower than that from the hydraulic testing data.

The final frequency comparison is the estimated frequencies from column (5) of Table 3.1 to the end of construction 10,000 day estimated design tensions. Table 4.8 shows the comparison of the frequencies to the plucked vibration data.

Table 4.8:Comparison of Frequencies from Plucked Data Frequencies and EOC 10,000 Tensions ($\bar{f}/f_{10k}$)

	Frequency Ratio ($\bar{f}/f_{10k}$)					
	Mode Number					
Cable	n=1	n=2	n=3	n=4	n=5	n=6
219E	-	0.9422	-	0.9422	-	0.9422
219E*	-	0.9348	-	0.9270	-	0.9321
319E	-	0.9068	-	0.9164	-	-
315E	-	0.9637	-	0.9499	-	0.9547
310E	1.0094	1.0094	1.021	-	-	-
305E	0.9274	0.9299	-	-	-	-
404E	0.9748	-	-	-	-	-
408E	0.9166	0.9324	0.9325	-	-	-
413E	0.8803	0.8911	0.9094	-	-	-
413E*	0.8955	0.9008	-	-	-	-

*Comparison of May 5th 2013 pluck test frequencies

Table 4.8 shows that the frequencies from the plucked test data have the weakest correlation to the EOC 10,000 loads. The range of the tensions in Table 4.8 is from 0.88 to 1.02, showing that almost all of the cables are below the EOC 10,000 design tensions. This is understandable because those design tensions are for almost thirty years after the end of construction and take into account creep from concrete and any other wearing surface added to the bridge deck.

This comparison of frequencies shows that the cable frequencies at the time of the plucked vibration test are most closely aligned with the estimated frequencies from the hydraulic jack measurements.

4.2.2 Tension Comparison

This section will be used to compare the design and measured hydraulic tensions to the tensions estimated from the plucked data frequencies found in Table 4.5. Table 4.9 is the comparison of the estimated tensions from the plucked vibration test to the end of construction loads. Each row is only compared to one tension as the increase in mode number compensates for the increase in frequency; in theory the tension at one mode should be the same at another as they are multiples of the fundamental frequency.

Table 4.9: Comparison of Plucked Vibration Tensions to EOC Tensions ($\bar{T}/T_{EOC}$)

	Tension Comparison ($\bar{T}/T_{EOC}$)					
	Mode Number					
Cable	n=1	n=2	n=3	n=4	n=5	n=6
219E	-	0.9366	-	0.9366	-	0.9366
219E*	-	0.9209	-	0.9215	-	0.8735
319E	-	0.8808	-	0.8997	-	-
315E	-	0.9940	-	0.9566	-	0.9755
310E	1.1237	1.1237	1.1506	-	-	-
305E	0.9079	0.9127	-	-	-	-
404E	0.9890	-	-	-	-	-
408E	0.8988	0.9300	0.9302	-	-	-
413E	0.8048	0.8247	0.8589	-	-	-
413E*	0.8318	0.8449	-	-	-	-

*Comparison of May 5th 2013 pluck test tensions

The comparison of estimated tensions from the plucked test to the end of construction loads shows that the tensions vary from 80% to 115% of the design end of construction loads. Cable 310E is the only estimated cable tension that is higher than its estimated design load; excluding that cable all of the other estimated tensions are below the end of construction design tension. Table 4.10 shows the ratio of the estimated tensions from the vibration data to the hydraulic jack measured tensions.

Table 4.10: Comparison of Plucked Vibration Tensions to Hydraulic Measured Tensions ($\overline{T}/T_{MH}$)

	Tension Comparison ($\overline{T}/T_{MH}$)					
Cable	n=1	n=2	n=3	n=4	n=5	n=6
219E	-	0.9359	-	0.9359	-	0.9359
219E*	-	0.9215	-	0.9066	-	0.9166
319E	-	0.9101	-	0.9295	-	-
315E	-	0.9953	-	0.9671	-	0.9768
310E	0.9517	0.9517	0.9745	-	-	-
305E	0.9001	0.9048	-	-	-	-
404E	0.8656	-	-	-	-	-
408E	0.8529	0.8825	0.8827	-	-	-
413E	0.8494	0.8704	0.9064	-	-	-
413E*	0.8778	0.8916	-	-	-	-

*Comparison of May 5th 2013 pluck test tensions

The difference between the tensions in Table 4.9 and 4.10 occur more in the shorter cables as the tensions in the longer cables does not change a significant amount from the EOC tensions and the hydraulically measured tensions. A possible reason for the small change in tension in the longer cables is that the loading scenario for the particular section of the bridge is not estimated to have a great change over the 10,000 day period. They are the furthest cables from the pylon and the deck profile and shape does not change very much at that distance. The range of tensions in Table 4.10 is 0.85

and 0.98 which are all lower than the measured tensions from the vibration testing. This is typical considering the tensions in this case are generally higher than those of the EOC design tensions. Table 4.11 shows the comparison of tensions from Table 4.8 to the EOC 10,000 tensions.

Table 4.11: Comparison of Plucked Vibration Tensions to Design EOC 10,000 Tensions ($\overline{T}/T_{10k}$)

	Tension Comparison ($\overline{T}/T_{10k}$)					
	Mode Number					
Cable	n=1	n=2	n=3	n=4	n=5	n=6
219E	-	0.8878	-	0.8878	-	0.8878
219E*	-	0.8765	-	0.8594	-	0.8688
319E	-	0.8223	-	0.8399	-	-
315E	-	0.9287	-	0.9024	-	0.9114
310E	1.0189	1.0189	1.0433	-	-	-
305E	0.8601	0.8647	-	-	-	-
404E	0.9503	-	-	-	-	-
408E	0.8401	0.8693	0.8695	-	-	-
413E	0.7749	0.7941	0.8270	-	-	-
413E*	0.8010	0.8135	-	-	-	-

*Comparison of May 5th 2013 pluck test tensions

The comparisons shown in Tables 4.9, 4.10, and 4.11 show that the tension in the cables will differ depending on the data in which tension measurements are taken.

Referring to Table 3.1, the tensions, in theory, should be increasing over time until they reach the EOC 10,000 design tensions. This appears to be happening in some of the longer cables but the shorter cables have shown a great deal of fluctuation in where they are in their individual tension progression. In 310E the loads measured from vibration data are 1% to 2% higher than the estimated EOC 10,000 loads. The design tensions that are given from the drawings are projected and subject to change, the tensions could be affected by change in deck profile, extra loads unknown when designing, and other factors. Even though the tensions fluctuate, in some cases higher than their projected design tensions, all of the measured loads are less than the estimated ultimate loads from the drawings. A better way of displaying how the measured tensions from the vibration testing compare to design and ultimate tensions is to show them graphically. Figures 4.13 and 4.14 show a graphical comparison of the ultimate tensions to the measured tensions from vibration testing and the estimated design tensions from the construction drawings. Figure 4.13 is the comparison of the ultimate maximum and minimum tensions to the estimated tensions ($\overline{T}$). The ultimate design maximum and minimum are the absolute largest and smallest tensions that the particular cable can handle. In relation to the design construction loads they are just the maximum and minimum tensions that the cables should ever face, the design tensions are lower for conservative measures. The ultimate tensions that are reported are from the same construction drawing as where the EOC and EOC 10,000 design tensions were pulled from.

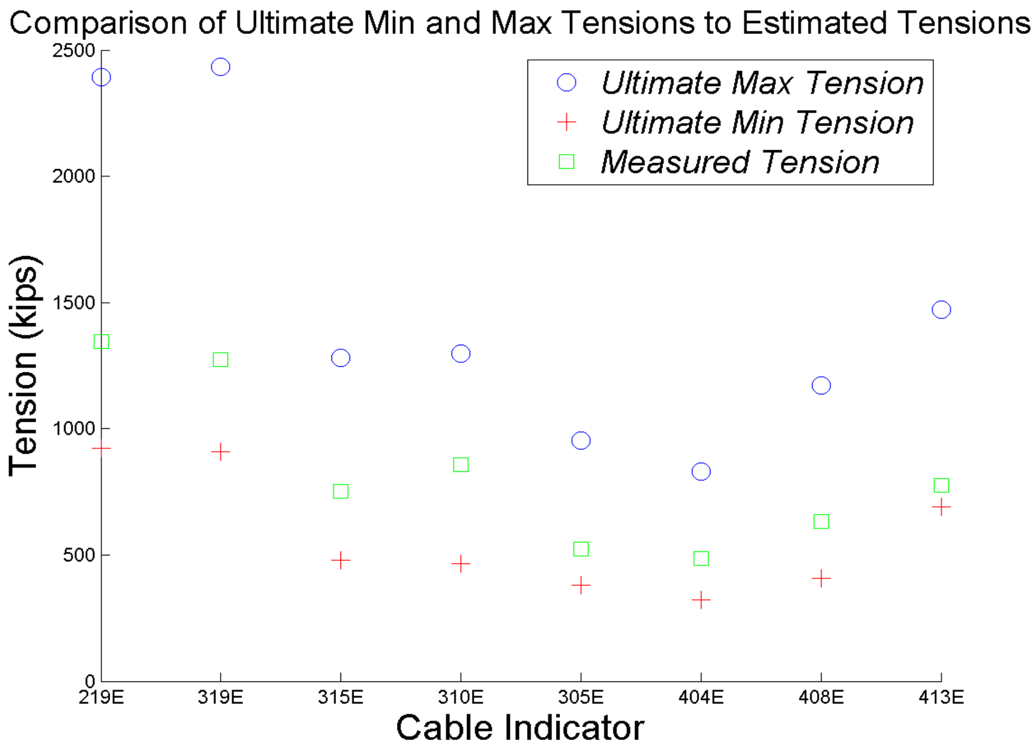

Figure 4.13: Comparison of Ultimate Max and Min to Estimated Tensions ($\bar{T}$)

Figure 4.13 shows that the measured tensions, green squares, are between the ultimate minimum and maximum of the design cable tensions. The Y axis is the cable tension and the X-axis is the stay designation. None of the west side cables or 419 East are graphed. Figure 4.14 is a comparison to the different estimated end of construction tensions.

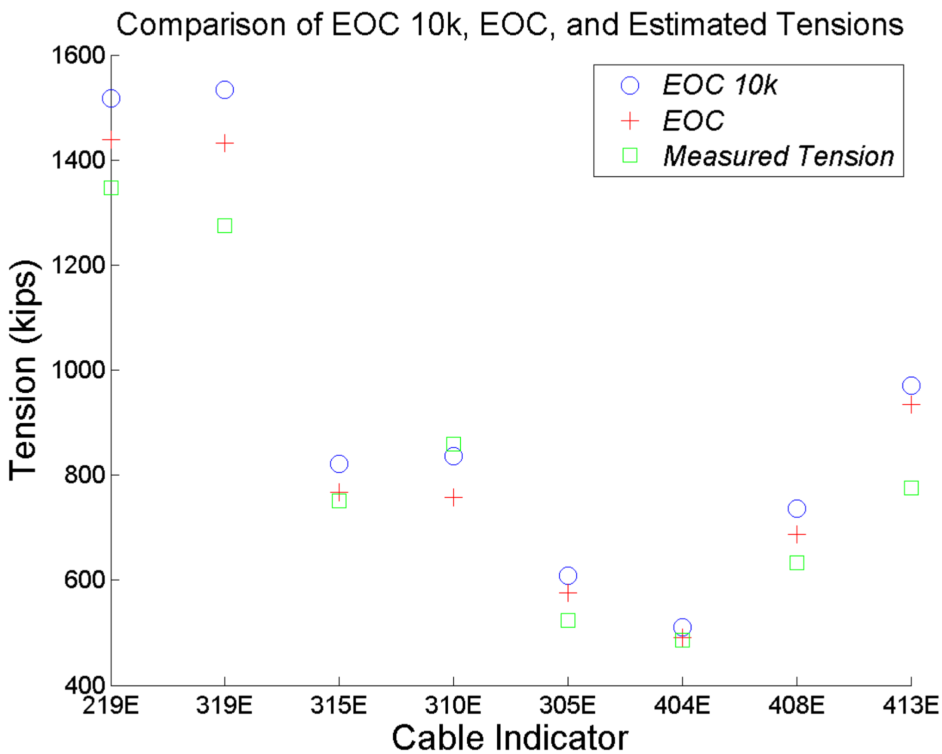

Figure 4.14: Comparison of EOC 10k (T_{10k}), EOC (T_{EOC}), and Estimated Tensions ($\overline{T}$)

Figure 4.14 is a visual representation of where the tensions compare to the two different end of construction load cases. The measured tensions graphical and tabular forms both show that accelerometer data can be used to predict the tensions in the cables. Furthermore, the solution to the simple taut cable theory equation, (1.4), is a fast reliable and practical method for quickly and accurately predicting the tension in the monitored cables on the Indian River Inlet Bridge. Not only is (1.4) a practical equation for estimating cable tensions, but the computer methods described in chapter three are also sensible for extracting, analyzing, and estimating the natural frequencies of vibration for the cables. Although this section shows the results of only one controlled vibration test the results for eight different cables initially prove that the methods previously described are applicable to the problem of indirectly estimating cable tensions.

Comparison of the first pluck test to the second pluck test data shows that 219E has less tension than it did from the first test. It also shows that 413E carries more tension than before in the first load test. Although there was a change in the tension carried by both of these cables the results are not drastic enough to cause concern for the cables health. The change can be attributed to change possible changed in settlement, change in deck profile, long term temperature effects, and a variety of environmental conditions.

Chapter 5

AMBIENT VIBRATIONS AND ALIASING

Unlike the previous chapter where the data was collected using forced controlled vibrations to get a response from the cables this section focuses on data collected from vibrations caused by wind excitations. This section looks at the problems associated with ambient vibration data and examples of ambient data.

5.1 Ambient Vibrations

One of the advantages of having the system constantly monitoring is that data can be collected during high wind events without anyone present. This helps with not only monitoring the behavior of the cables during these events but can also provide frequencies that can be used to estimate cable tensions.

The data that will be presented in this section is from vibrations due to hurricane Sandy that struck the Delaware coast in October 2012 between the 28th and 30th. According to the Delaware Environmental Observing System website, which monitors and records environmental data for the area, the maximum average wind speed over at 5 minute period was 38.8 mph and the maximum wind gust speed was 46.9 mph. The data analyzed is taken from a sample on October 28that 4:35 pm, with approximate average wind and gust speeds of 27.9 mph and 31.7 mph, respectively (DEOS website). The winds for this sample are just below the average wind and gust speeds recorded over the length of the hurricane event. The duration of the data being collected was 10 minutes set by the user on the system at a rate of 125 Hz. Figures 5.1

to 5.11 show the power spectra from the data recorded for both sensors at that time. The MATLAB “cpsd” input parameters include a periodic hamming window (default for the cpsd function), a sample overlap of 2^{10} or 1,096 samples, and a Fast Fourier Transform length of 2^{11} or 2,048 samples. The top graph shows the data from the Y-direction sensor and the bottom graph shows the data from the Z-direction sensor. The frequency is capped at 45 Hz as most frequencies outside of 20 Hz are not used in estimating the stay tension.

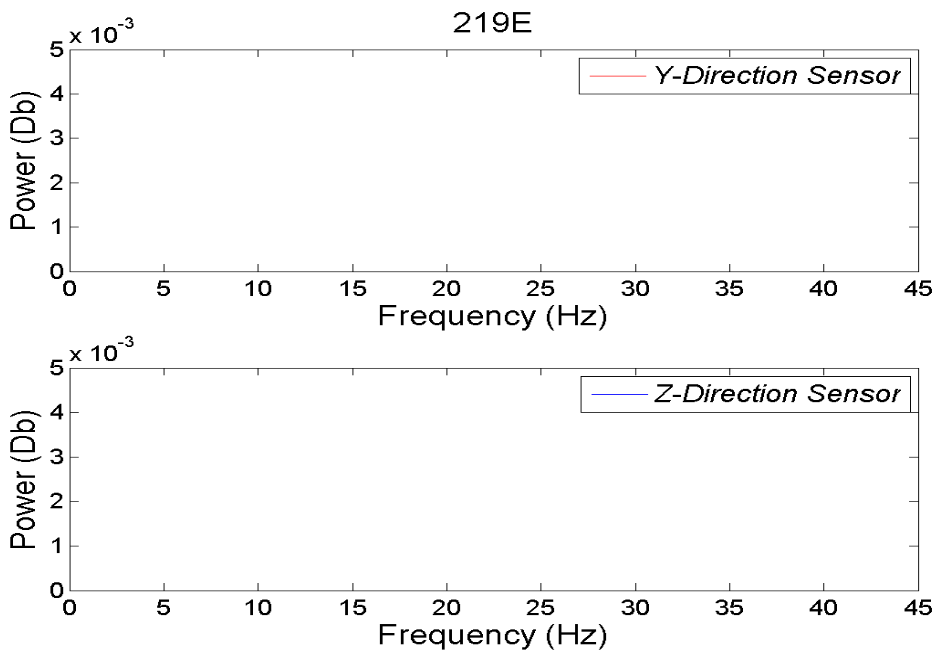

Figure 5.1: Ambient Data for 219E

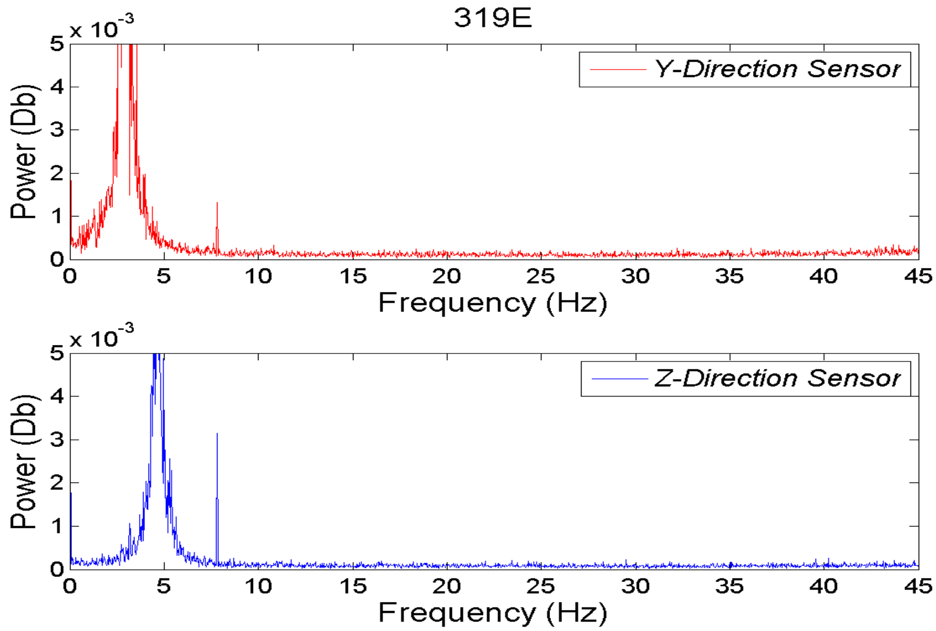

Figure 5.2: Ambient Data for 319E

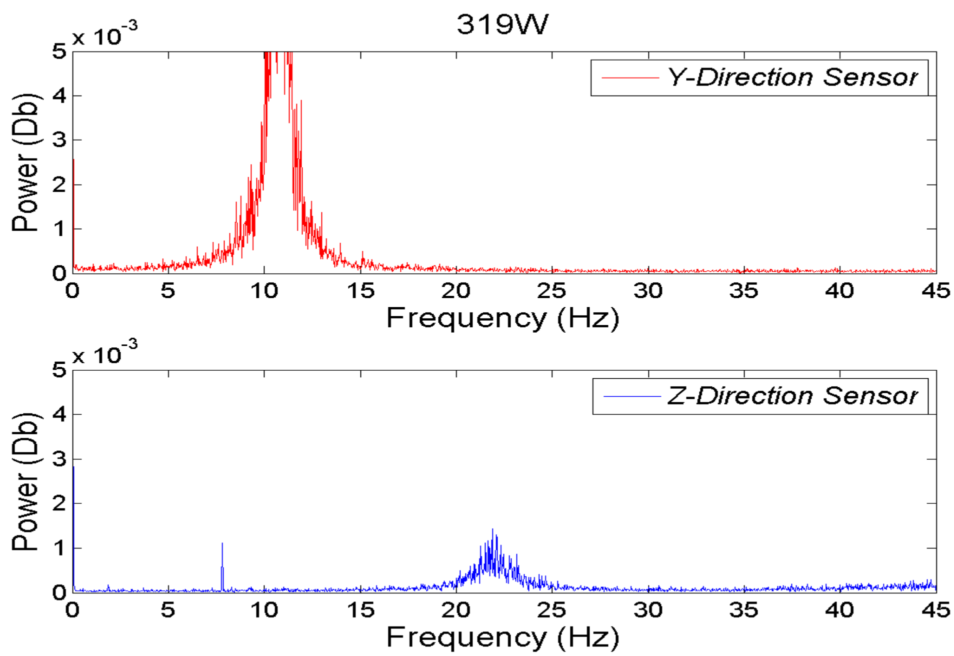

Figure 5.3: Ambient Data for 319W

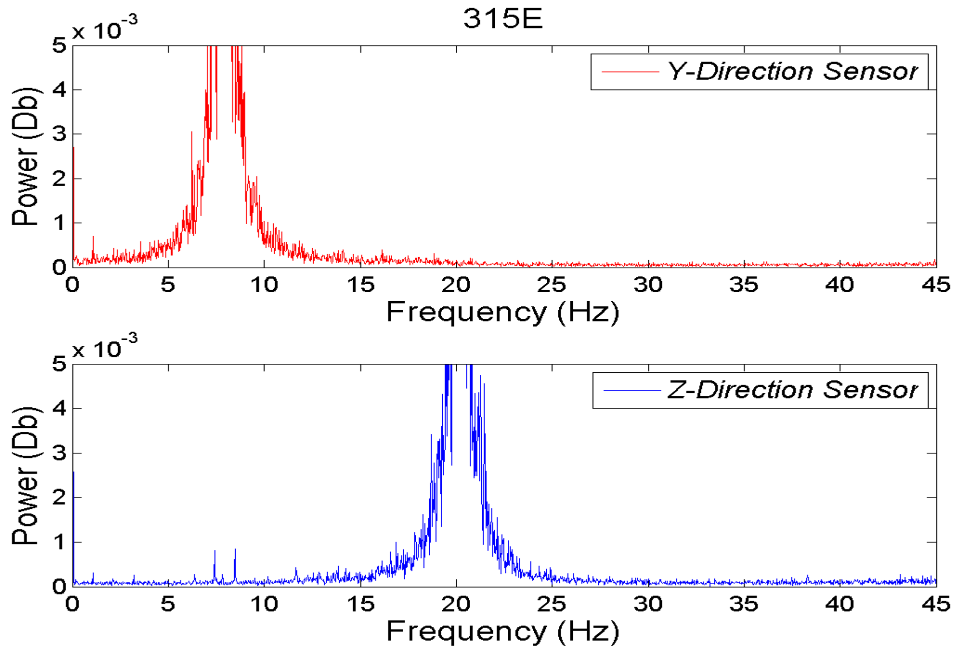

Figure 5.4: Ambient Data for 315E

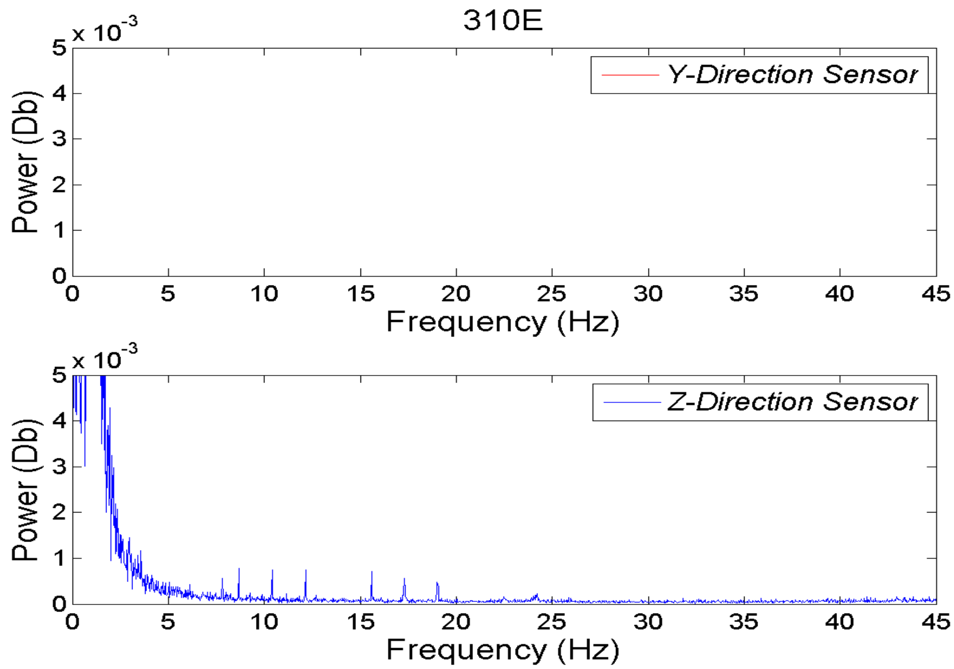

Figure 5.5: Ambient Data for 310E

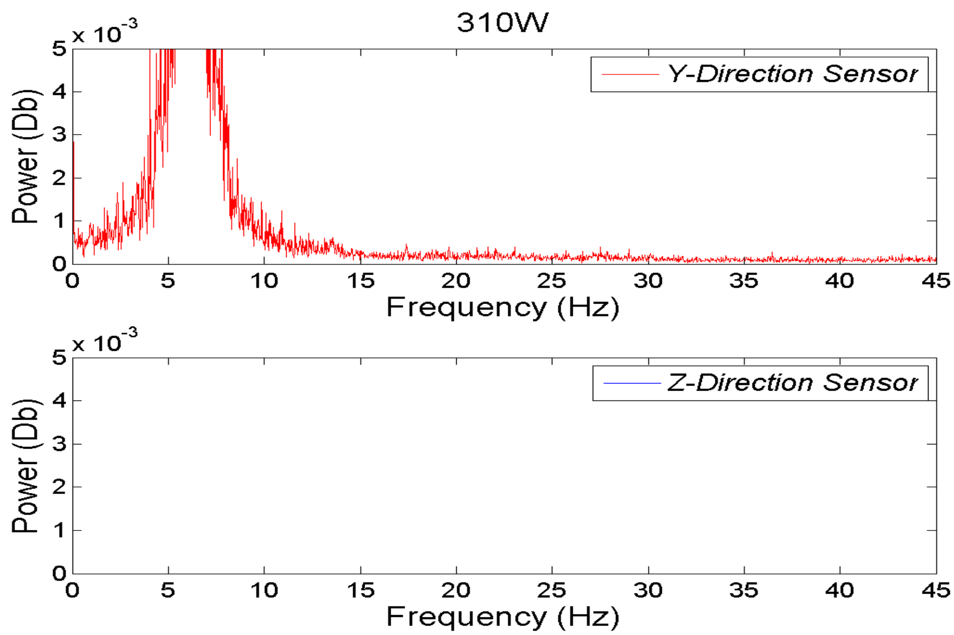

Figure 5.6: Ambient Data for 310W

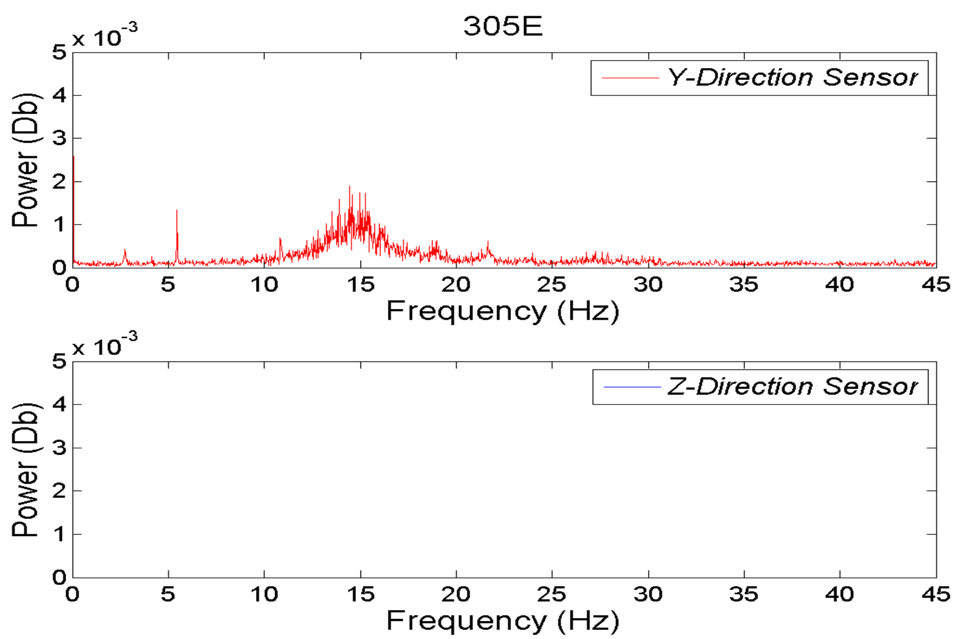

Figure 5.7: Ambient Data for 305E

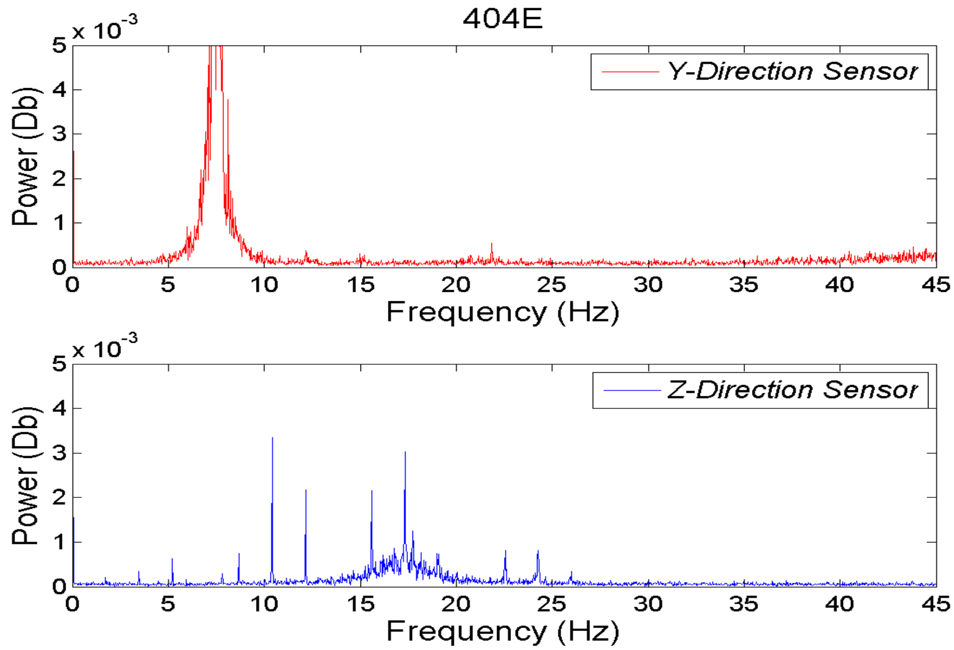

Figure 5.8: Ambient Data for 404E

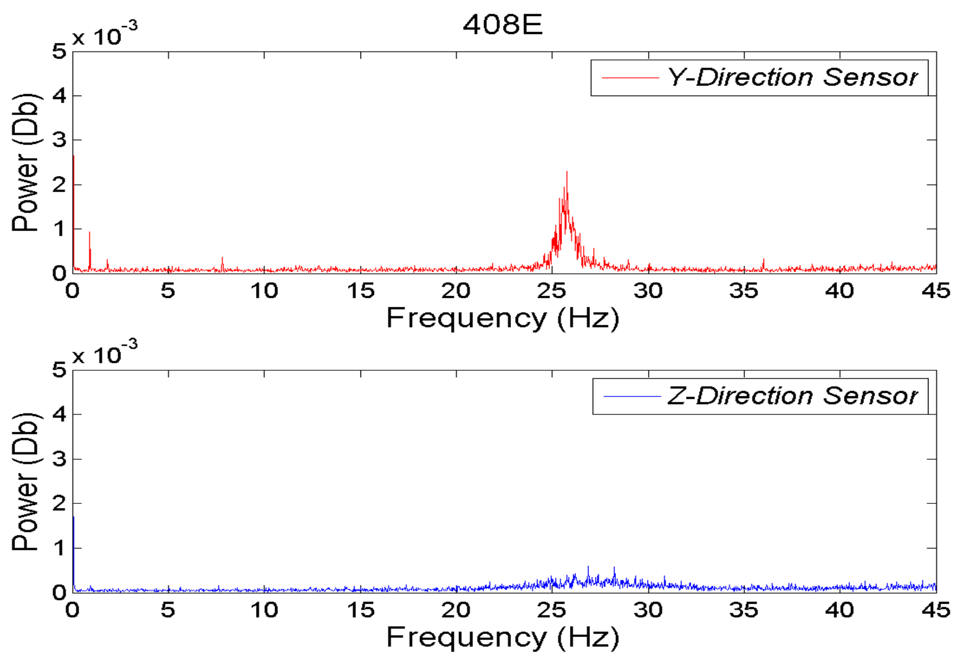

Figure 5.9: Ambient Data for 408E

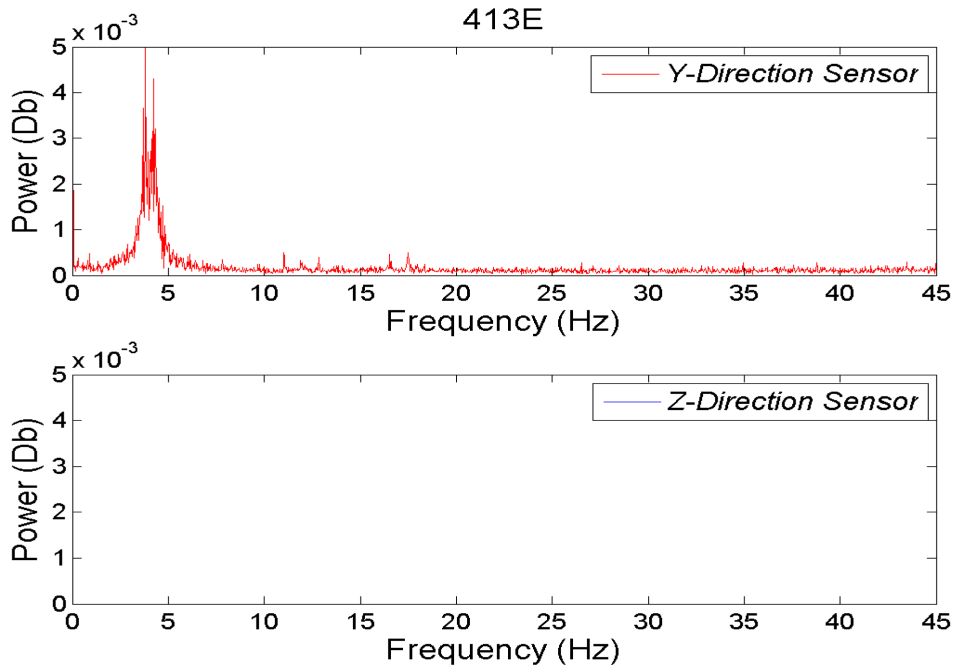

Figure 5.10: Ambient Data for 413E

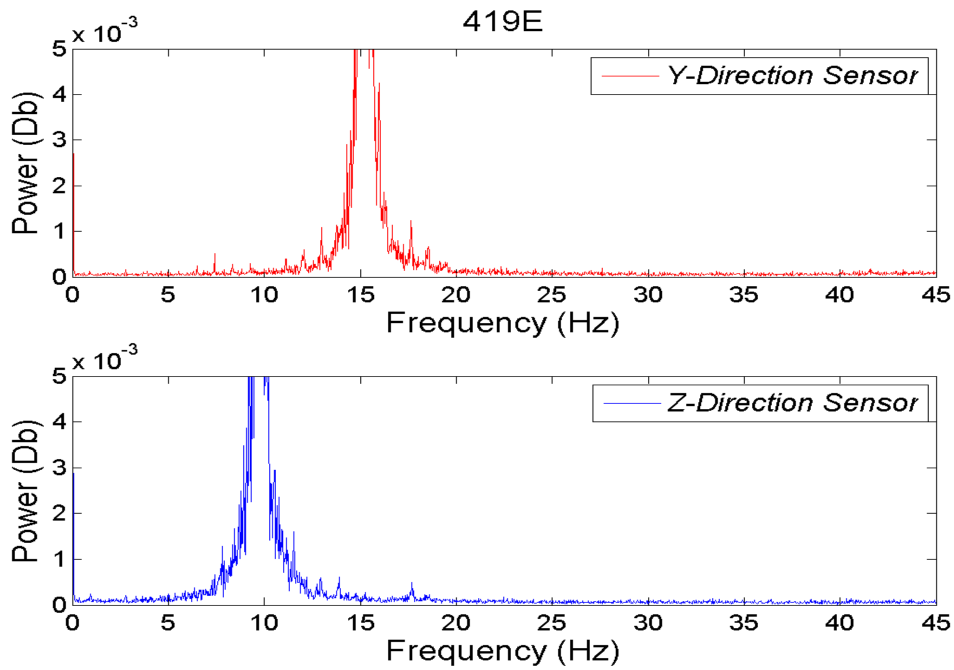

Figure 5.11: Ambient Data for 419E

The figures give insight to the applicability of using ambient field vibration data. Some of the graphs do not show any data, which simply means that the sensor either did not display data or was not working at the time. These sensors include both 219E sensors, 310E Y direction sensor, 310W Z direction sensor, 305E Z direction sensor, and 413E Z direction sensor. For almost all of the sensors there is a wide band, strong peak in the power spectra that is not believed to be associated with a natural frequency of the stay, but is believed to be due to aliasing of the sensor natural frequency folding down into the lower frequency range. In some cases the aliasing dominates the signal in low frequency ranges where the stay fundamental frequencies are expected to be found.

Signal aliasing occurs when higher frequencies, like the resonant frequency of the sensors, fold down and appear as a lower frequency in a spectra (National Instruments 2006). Higher frequencies are considered any frequencies that are above the Nyquist frequency , which is equal to half of the sampling rate. The Nyquist frequency is usually used to find adequate sampling rate for oversampling and to try and avoid aliasing. Frequencies become indistinguishable because higher frequencies will "fold" over the Nyquist frequency and appear in lower frequency ranges. For example, if the sampling rate for a signal is 125 Hz the Nyquist frequency is 62.5 Hz. Any frequency that is greater than 62.5 Hz will fold over that frequency and appear as a lower frequency in the spectra. For example, in this case, a frequency of 80 Hz will appear at 45 Hz in the spectra. Frequencies greater than the sample rate will fold down to a lower frequency, according to the relationship seen in equation (5.1)

$$f_n = |f - Nf_s| \tag{5.1}$$

This is the basic aliasing equation in which f_s is the sampling rate, f is the frequency being sampled, in this case the resonant frequency of the sensor, f_n is the aliased signal, and N is the nearest integer of the ratio f/f_s. For example, a sampling frequency of 125 Hz a frequency of 140 Hz will fold to a frequency of 15 Hz. With the same sampling rate a frequency of 400 Hz will fold to 25 Hz. Conventional analog data acquisition systems use low-pass anti-aliasing filters to suppress any frequencies above the Nyquist frequency so that aliasing does not occur. The fiber-optic SHM system does not employ anti-aliasing filters.

The Micron Optics OS7100 accelerometers have a natural frequency of approximately 700 Hz (the exact natural frequency varies for each sensor). Therefore, according to equation (5.1), for a sample rate of 125 Hz, the 700 Hz natural frequency will appear at 50 Hz in the spectra (N=6). Likewise, at a sample rate of 250 Hz, the 700 Hz natural frequency will appear in the range of 50 Hz in the spectra (N=3). There will however be slight variations on this because the natural frequencies of the sensors are all unique. Referring to Figures 5.1 through 5.11, this is exactly the range in which the wide band, strong signal is present (most of the strong signals are below 50 Hz which implies that the natural frequencies of the mounted sensors are closer to 750 Hz than to 700 Hz).

Signal aliasing is a problem for this study because at certain sampling rates the resonant frequency of the sensor is folding into low frequency ranges and swamping the stay natural frequency peaks. This renders certain frequencies difficult to identify making any data in the aliasing range unreliable and therefore impractical for estimating that cables tensions.

In some of the sensors there are obvious frequency peaks that are unaffected by aliasing. For example, the power spectra for sensors 310E in the Z direction (Figure 5.5) and 404E in the Z direction (Figure5.8) have very noticeable peaks that can be identified and used to estimate tensions. Below in Table 5.1 are frequencies extracted from Figure 5.1 to 5.11 and organized by estimated mode number. In some cases the first frequency peak that is used is similar to the estimated fundamental frequency from the end of construction loads, f_{EOC}. From the f_{EOC} fundamentals frequencies the other modes can be estimated.

Table 5.1: Frequencies and Estimated Mode Numbers for Ambient Vibration Data ($\bar{f}_A$)

	Frequencies (Mode Numbers)										
	n=1	n=2	n=3	n=4	n=5	n=6	n=7	n=8	n=9	n=10	n=11
219E	NO PEAKS										
319E	NO PEAKS										
319W		1.862						7.813			
315E	1.068		3.204			6.378		8.484			
310E	7.813				8.667	10.41		12.15		15.59	17.3
310W	NO PEAKS										
305E	2.747	5.463									
404E	3.479	5.219	8.667	10.41		12.15	15.59				
408E	1.831			7.813							
413E							11.02	11.9	12.85		
419E	NO PEAKS										

These frequencies were then compared to the end of construction load frequencies as seen below in Table 5.2, ($\bar{f}_A/f_{EOC}$).

Table 5.2: Comparison of Ambient Frequencies to EOC Frequencies ($\bar{f}_A/f_{EOC}$)

	Frequency Comparison										
	n=1	n=2	n=3	n=4	n=5	n=6	n=7	n=8	n=9	n=10	n=11
219E	NO PEAKS										
319E	NO PEAKS										
319W		0.969						1.016			
315E	0.997		0.997			0.992		0.99			
310E					1.075	1.076		0.942		0.967	0.98
310W	NO PEAKS										
305E	0.974	0.969									
404E	1.181	0.886	0.981	0.883		0.825	0.882				
408E	0.981			1.046							
413E							1.079	1.019	0.979		
419E	NO PEAKS										

Comparing Table 5.2 to Table 4.6 shows that the measured ambient vibration frequencies are similar to the frequencies collected from the pluck test. One of the more obvious differences between $\bar{f}$ and $\bar{f}_A$ is that the ambient data provides higher order frequencies of vibration. In the plucked cases the highest recordable frequency peak was at n=6 where in the ambient case the highest mode recordable was the 11th mode. The ambient data shows that the system is capable of picking up different frequencies for different excitation events. This shows the flexibility of the system to pick up not only the first few fundamental frequencies but higher order frequencies. Having the option to use high mode numbers for vibration is useful in a case where the exciting force may excite only certain modes of vibration. In the plucked vibration tests there was little presence of aliasing but in the ambient vibration case the aliasing is much more obvious and prevalent. Below in Table 5.3 is an extension of Table 5.1 and presents the aliasing ranges that appear in the ambient vibration data.

Table 5.3: Aliasing Ranges for Ambient Vibration Data

	Aliasing Range	
	Y	Z
219E	SENSOR OUT	
319E	0-6 Hz	NO DATA
319W	6-14 Hz	20-25 Hz
315E	4-11 Hz	15-25 Hz
310E	NO DATA	0-5 Hz
310W	0-11 Hz	NO DATA
305E	10-20 Hz	NO DATA
404E	5-10 Hz	15-20 Hz
408E	25-30 Hz	25-27 Hz
413E	3-7 Hz	NO DATA
419E	11-18 Hz	6-11 Hz

When comparing the aliasing ranges shown in Table 5.3 to other aliasing ranges from other Hurricane Sandy records it was found that the aliasing range is consistent for each respective sensor. This shows that the aliasing will occur at the same frequencies for different high wind events; typically the only difference is the power of the aliased frequencies.

Chapter 6

CONCLUSIONS AND FINAL ANALYSIS

This section will summarize the research and the systems use moving forward. Also, a discussion of complications associated with the system as well as final conclusions about the system and recommendations for the future.

6.1 Conclusions

This study has shown not only the benefits but also the limitations of fiber optic sensors and an optical system. The study has also explored multiple dynamic cable equations that could be used to measure the tension from acceleration data. This section will be used to summarize and draw conclusions about the data presented in previous chapters.

The most important conclusion is that the fiber-optic accelerometers used to gather data in this study are sufficient for recording raw acceleration data from the cables when excited. Also, the accelerometers are an excellent substitute for other more complicated testing methods as well as a viable solution for long term structural health monitoring of the Indian River Inlet Bridge cable stays.

The data processing methods selected for extracting, organizing, and evaluating the accelerometer are MATLAB script files for extracting and evaluating, and a built in power spectra function in MATLAB for evaluating the data. The power spectra of the acceleration data is the most applicable way to extract frequencies without having to do meticulous period counts for each data set. Using the CPSD function in a MATLAB script file in combination with other data processing commands the data is easily taken from acceleration time history data and converted into the frequency domain where frequencies can be more easily found.

The methods for estimating tensions that were described in Chapter 2 are not necessarily worse than the equation used for estimating tension in this study. The accuracy that is gained from using more precise methods is comparable to the extra time or processing memory to use more complex methods. For example, the comparison of the tension results from equation (1.4) and the solution to equation (1.1) is less than one kip difference. The methods that include sag and bending stiffness simply are applicable for the cables. The cables cross sectional stiffness are too small for cross sectional stiffness to play a factor. In the case of sag, the length to tension ratio is far too low to have considerable changes in tension. Also, the relatively low length to tension ratio eliminates the possibility of an avoided crossover and dynamic amplification factor. Calculating the sag parameter for the cables using equation (2.1) yields a maximum number of 0.2, which is considered extremely low sag. Iterative and finite element methods are the most accurate but are also the most time consuming. For the purposes of this study neither was considered necessary considering extreme accuracy is not imperative.

The results presented in Chapters 4 and 5 demonstrate that the data produced from the sensors can be processed and used to identify frequencies that result in reasonable tensions. Figure 4.14 shows that the estimated pluck test tensions are similar to the end of construction design tensions. The tensions from the pluck test range from 1347 kips to 486 kips, compared to the end of construction range of 1438 kips to 486 kips. The largest negative difference in tension was in cable 319E, which was 157 kips lower than the design tension (1432 kips EOC). It should also be noted that cable 413E was 155 kips lower than the end of construction design tension (934 kips EOC). The largest positive difference was in cable 310E, which was 101 kips greater than the end of construction design tensions (758 kips EOC). With the exception of cable 310E, all other cable tensions were lower than the end of construction design tensions. Referring to Figure 4.13, the pluck test tensions are within the ultimate maximum and minimum ranges from the construction drawings. Commenting on the difference between the measured tensions and the end of construction tensions, the tension in the cable can change due to a variety of factors including: truck traffic, temperature, expansion and contraction of the deck, wind, and deck profile. When assessing the accuracy of the sensors and computer methods, the tension comparison results in Tables 4.9 and 4.11 shows that 0.78 and 1.12 are the minimum and maximum ratios of the pluck tensions to the end of construction design tensions. Looking at the comparison of the pluck test to the hydraulically measured tensions in Table 4.10 it is seen that the range is 0.85 to 0.97 meaning that the pluck test tensions agree well with the hydraulically measured tensions. The comparison in Table 4.10 proves that the basic cable equation is a fast, accurate method to get a tension measurement.

Chapter 5 shows the capabilities of the sensors when measuring ambient vibrations of the cables when excited by wind. The range of the frequencies over different mode numbers is much greater than that of the plucked vibration tests. The highest value found in the plucked vibration tests was the 6th mode where in the ambient vibration test up to the 11th mode was recorded in some cases. In general higher mode numbers were found in the ambient vibrations. This can be expected considering the exciting force of the wind was not characterized and could easily have excited higher modes. From the ambient data it is important to understand that although, some of the sensors did not record peaks, the sensors are capable of recording data that produces obvious frequency peaks. A good comparison would be to compare Tables 4.6 and 5.2, they both compare frequencies to the end of construction loads. Taking the average ratio for each cable yields a range of 0.913 to 1.064for the plucked frequencies compared to EOC frequencies. Taking the average from the frequencies in Table 5.2 gives a range of 0.891 to 1.026, a difference of 0.022 and 0.038 respectively, showing that the ambient frequencies are close to the ones gathered in the plucked tests. This shows that recording ambient vibrations is an adequate method to get quick accurate tension results. Even though it has been stated that most of the dynamic tension is contributed from the first few fundamental frequencies, calculating the tension using higher modes is just an extension of the first fundamental frequency. Using the concept that higher frequencies are multiples of the first frequency calculating tension from higher frequencies is an acceptable and accurate way to estimate tensions. Comparison of Chapter 5 results to analogous results in Chapter 4 show that ambient vibrations like plucked vibrations can and should be used to measure the tension of the cables on the Indian River Inlet Bridge.

Overall this study has proven a number of important questions about long term structural health monitoring of the cable stays on the Indian River Inlet Bridge. First, the sensors that are being used on the cables are adequate at measuring and recording ambient and plucked type vibrations. Second, the MATLAB script file and power spectra used to process the vibration data are fast and effective at converting acceleration time history data into the frequency domain. Finally, the basic vibrating dynamic cable equation, (1.4), is the most practical method for quickly and accurately estimating tensions from frequency data.

6.2 System Complications

6.2.1 Ambient Data Problems

As seen in Figure 3.9 the sensors are mounted on a plate that is attached to the cable sheath and not directly to the cable strands themselves. This may cause a problem with sensitivity of the sensors to small vibrations in the cables. If the cable is not excited to a point where the sensor can pick up the vibration on the outside of the cable the sensor will record data that looks like the data in Figure 6.1. The Y axis is the cable accelerations in g's and the X axis represents time.

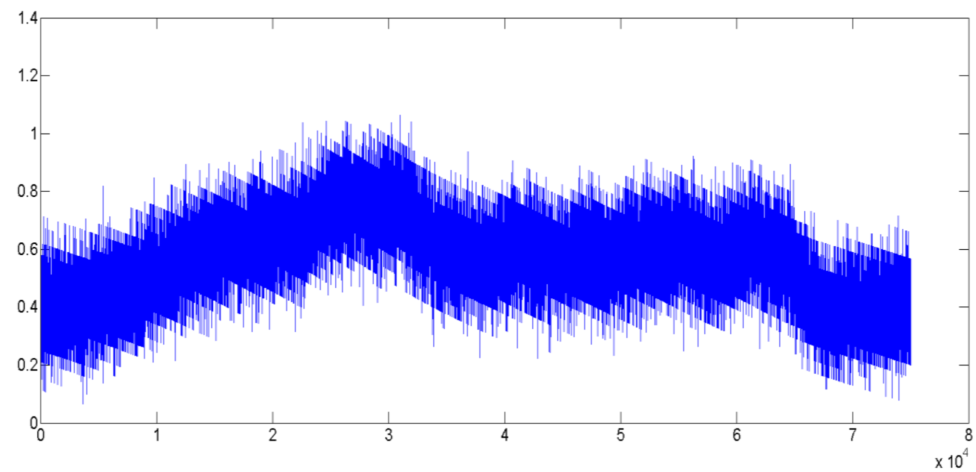

Figure 6.1: Example of Data with Small Accelerations

Figure 6.1 shows acceleration data where the sensor was unable to pick up recordable accelerations. The power spectra of the signal is a simply a flat line with no frequency peaks. For light wind events or in any case where the displacement of the cable is not adequate enough to excite the fundamental frequencies the sensitivity of sensors needs to be adjusted. A high wind event or a shake test would also be adequate to estimate the tension in the cables.

6.2.2 Possible Solutions to Aliasing

Signal aliasing occurs more in the ambient vibration data. Although aliasing presented problems in that analysis of ambient vibration data, some of the data from certain cables was usable for estimating tensions. Also, there are solutions to the aliasing issue that are common practice. For many sensors that are used in the field where aliasing could be an issue they have an anti-aliasing filter which is built into the sensor itself. At Indian River the sensors could either be retro-fitted or replaced with accelerometers that have built in anti aliasing filters. Whether the retro-fitting is possible or sensor replacement is even practical has yet to be determined but the associated cost and time of replacing or repairing the current accelerometers would suggest it to be unreasonable. Another possible approach that does not require altering or replacing the sensors is changing the sampling rate of the system. For most of the data collected the sample rate has been 125 Hz or 250 Hz which create aliasing where the estimated fundamental frequencies would be. The idea behind changing the sampling rate is that the folding will still occur but the folded signal will be outside of the 0-25 Hz range.

Using the Micro Optics recommended operating resonant frequency around 700 Hz and using a range of 680-720 Hz, sampling frequencies that keep the aliasing range out of the 0-25 Hz range. The estimated frequencies that can be used are 150-160 Hz, 190-210 Hz, 270-300Hz, and various high sampling rates like 333 Hz, 500

Hz, and 1 kHz. The higher sampling rates are impractical as the amount of data in a file with a sampling rate as high as 333 Hz would be very time consuming. One sensor at even 150 Hz for 10 minutes produces 90,000 data points, for every cable accelerometer, 22, its roughly 2 million data points. With high sampling rates come larger data files which take more time to load and process.

6.3 Future Research

This study is the groundwork moving forward for the fiber optic sensing system and estimation of tensions in the cables. Once the system is calibrated correctly to measure small cable vibrations and the sampling frequency is set to avoid aliasing the sensors and system, in theory, will be able to provide estimations of cable tension at any time. The computer codes can be refined to process and automate them to remove most if not all user interaction and could run in a shorter amount of time.

REFERENCES

Delaware Environmental Observing System (2013). "Inidan River Inlet, DE-LS Station." http://www.deos.udel.edu/ (October, 2012).

Irvine, H. K., and Caughey, T. K. (1974). "The Linear Theory of Free Vibrations of a Suspended Cable." *Proceedings of the Royal Society,* 299-315.

Kim, B. H., and Park, T. (2007). "Estimation of cable tension force using the frequency-based system identification method." *J.Sound Vibrat.,* 304(3-5), 660-676.

Kim, B. H., Park, T., Shin, H., and Yoon, T. (2007). "A Comparative Study of the Tension Estimation Methods for Cable Supported Bridges." *Ijss,* 7(1), 77-84.

Micron Optics. (2010). "Optical Sensing Interrogator SM130." http://www.micronoptics.com/uploads/library/documents/Datasheets/Micron%20Optics%20sm130.pdf (February 18, 2013).

Micron Optics. (2009). "Channel Multiplexer SM041." http://www.micronoptics.com/uploads/library/documents/Datasheets/Micron%20Optics%20sm041.pdf (March 3, 2013).

Mircon Optics. (2009). "Accelerometer OS7100." http://www.micronoptics.com/uploads/library/documents/Datasheets/Micron%20Optics%20os7100.pdf (February 15, 2013).

National Instruments. (2006). "Aliasing and Sampling at Frequencies Above the Nyquist Frequency ." http://www.ni.com/white-paper/3000/en/ (January 23rd, 2012).

R. Sexton, S. Koganti, A. Helmicki, V. Hunt, J. Swanson. (2005). "Aspects of Health Monitoring for Cable Stay Bridges." *Rep. No. 1,* University of Cincinnati Infrastructure Institute, University of Cincinnati.

Russell, J. C., and Lardner, T. J. (1998). "Experimental Determination of Frequencies and Tension for Elastic Cables." *Journal of Engineering Mechanics,* 124(10), 1067-1072.

Triantafyllou, M. S., and Grinfogel, L. (1986). "Natural Frequencies and Modes of Inclined Cables." *Asce*, 112(1), 139-148.

Zui, H., Shinke, T., and Namita, Y. (1996). "Practical formulas for estimation of cable tension by vibration method." *J.Struct.Eng.-ASCE*, 122(6), 651-656.

Appendix A

PLUCK VIBRATION GRAPHS

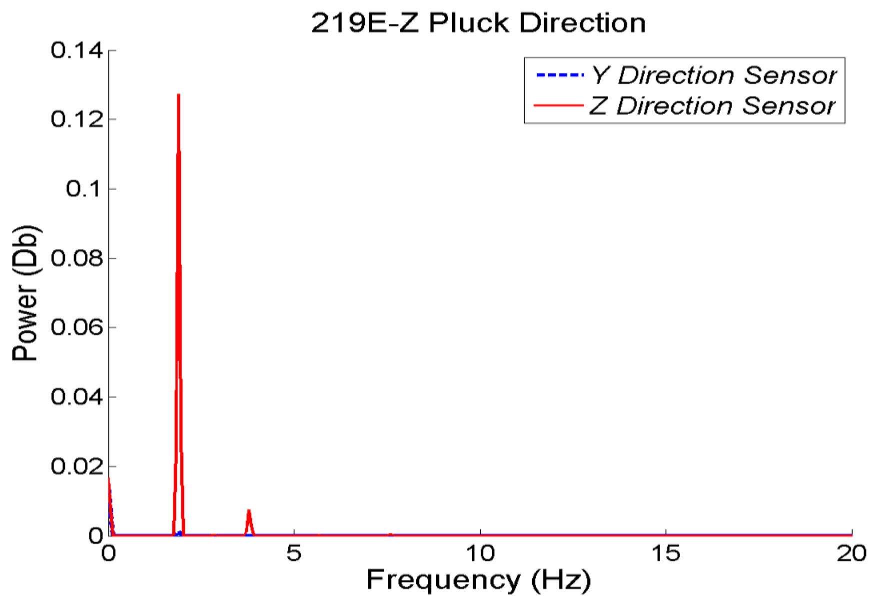

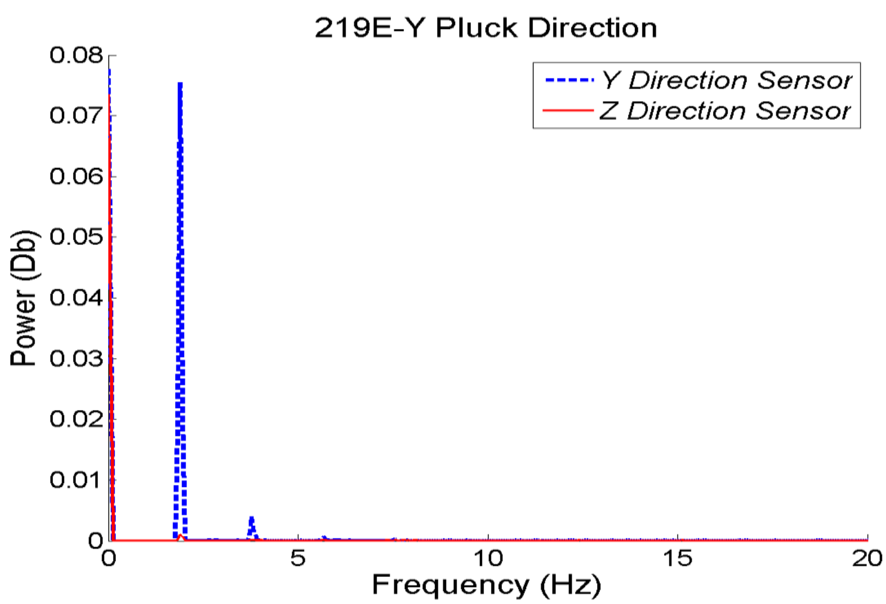

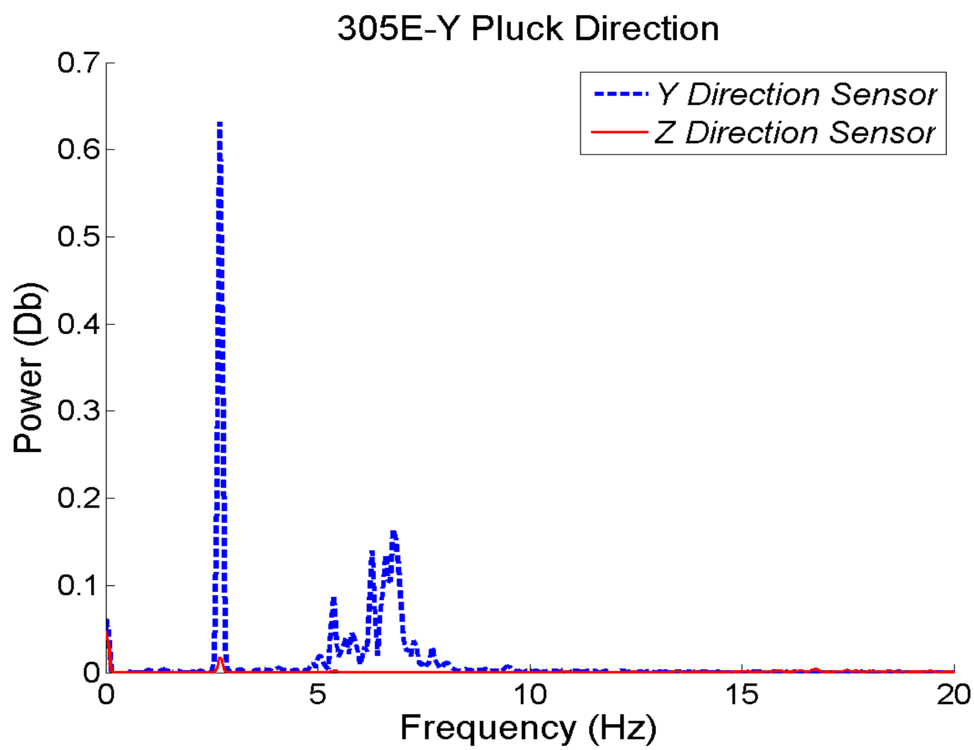
305E-Y Pluck Direction
Y Direction Sensor
Z Direction Sensor
Power (Db)
0
0.1
0.2
0.3
0.4
0.5
0.6
0.7
0
5
10
15
20
Frequency (Hz)

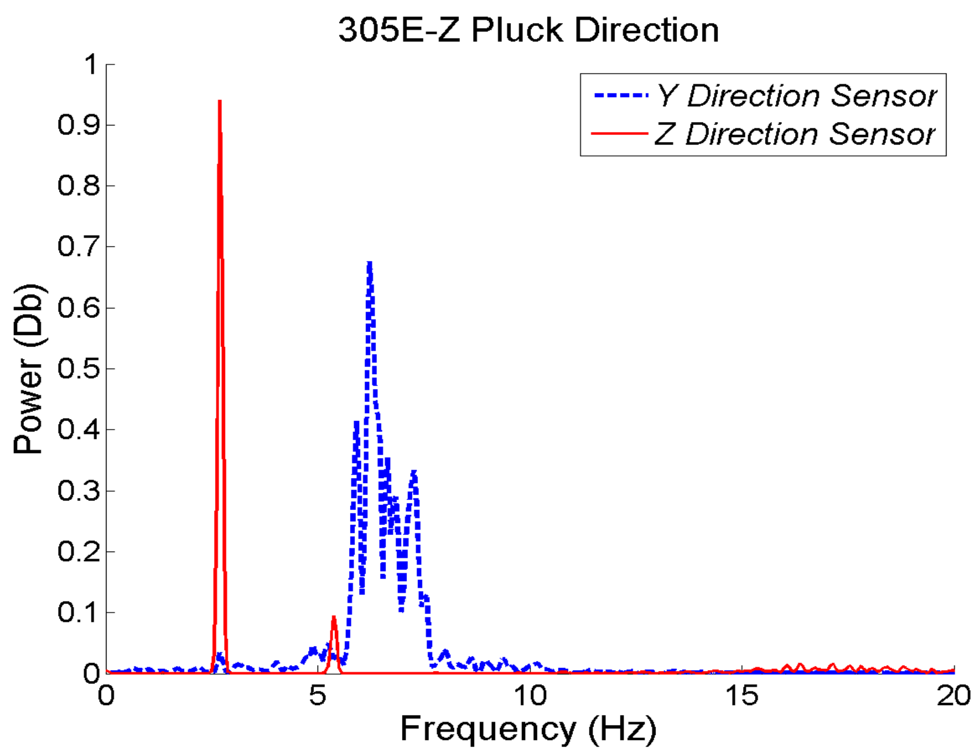
305E-Z Pluck Direction
Y Direction Sensor
Z Direction Sensor
Power (Db)
0
0.1
0.2
0.3
0.4
0.5
0.6
0.7
0.8
0.9
1
0
5
10
15
20
Frequency (Hz)

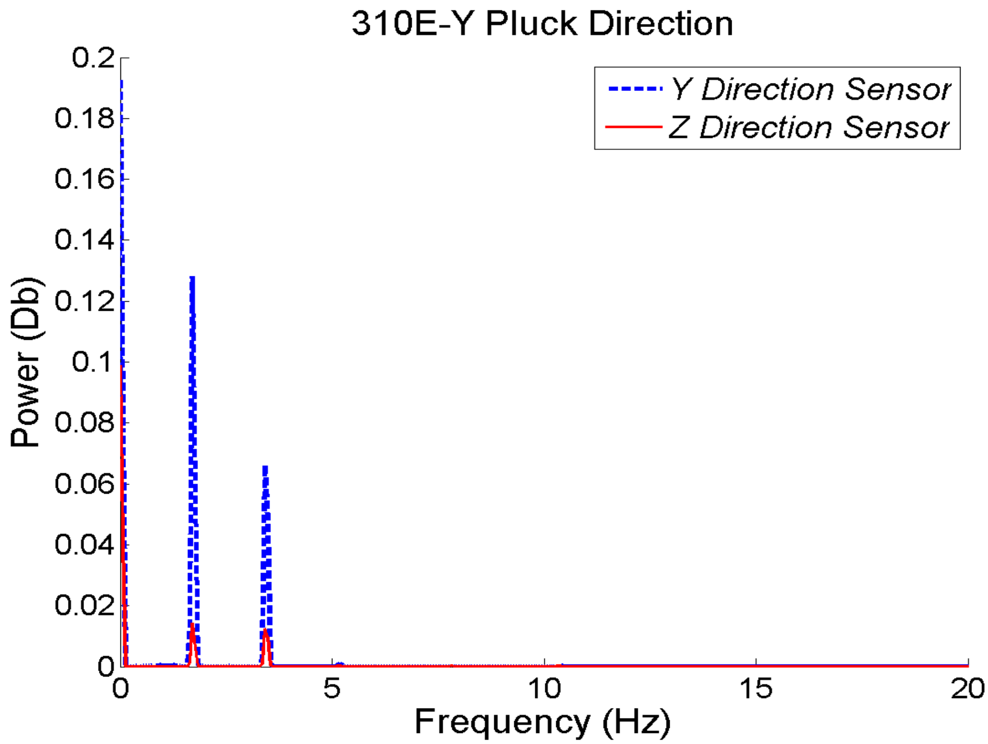
310E-Y Pluck Direction
Y Direction Sensor
Z Direction Sensor
Power (Db)
0.2
0.18
0.16
0.14
0.12
0.1
0.08
0.06
0.04
0.02
0
0
5
10
15
20
Frequency (Hz)

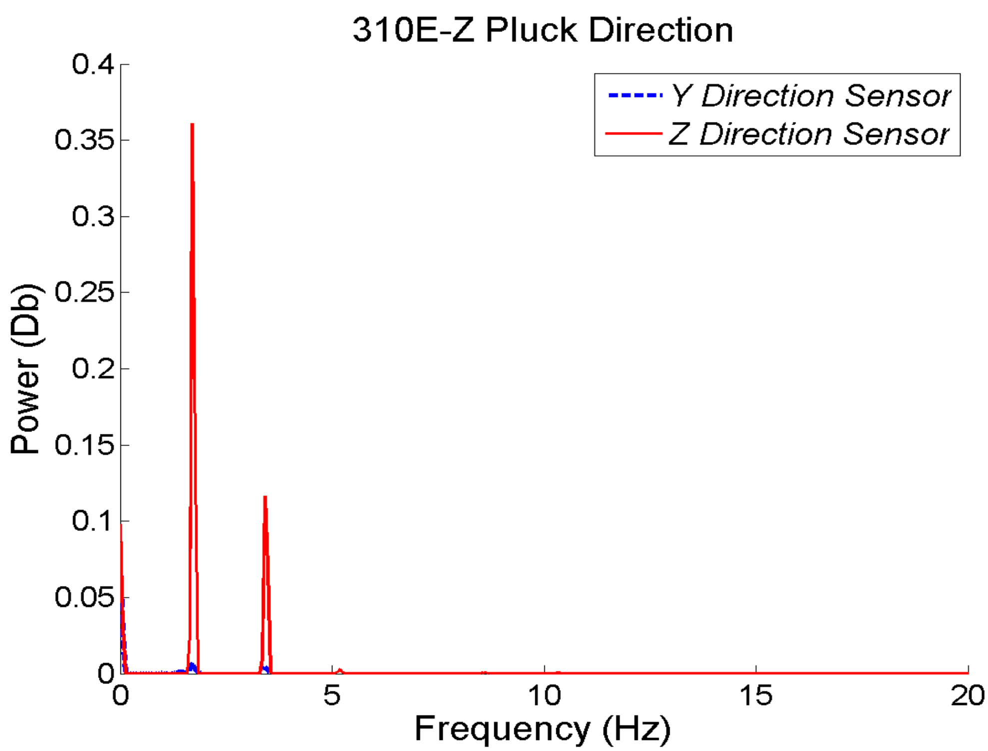
310E-Z Pluck Direction
Y Direction Sensor
Z Direction Sensor
Power (Db)
0.4
0.35
0.3
0.25
0.2
0.15
0.1
0.05
0
0
5
10
15
20
Frequency (Hz)

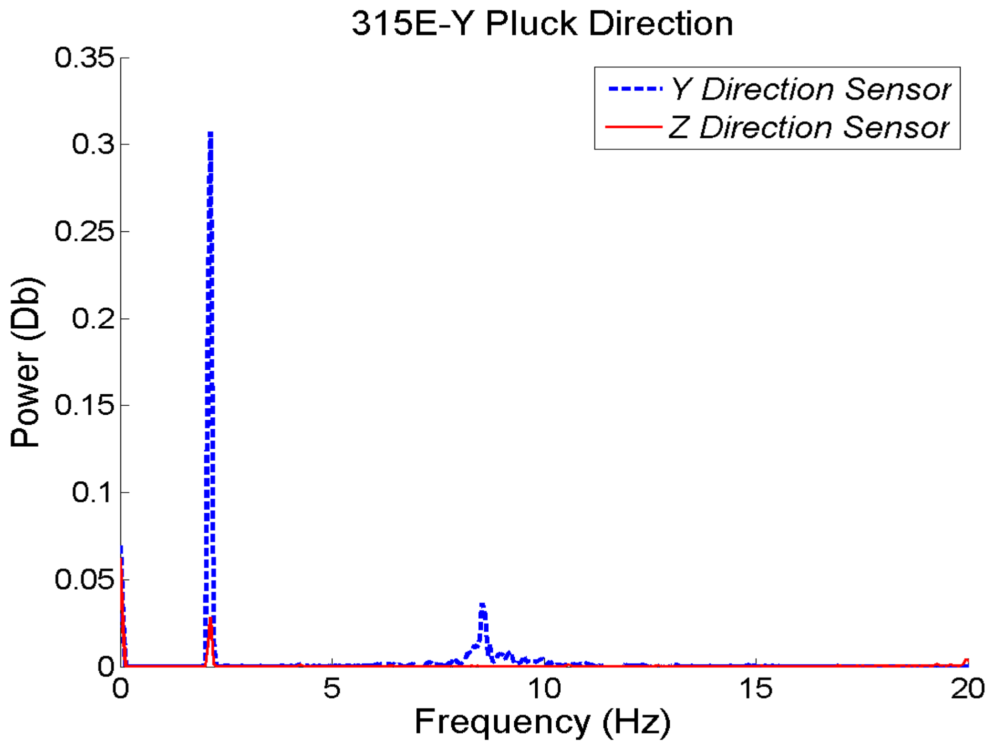
315E-Y Pluck Direction
Y Direction Sensor
Z Direction Sensor
Power (Db)
Frequency (Hz)
0.35
0.3
0.25
0.2
0.15
0.1
0.05
0
5
10
15
20

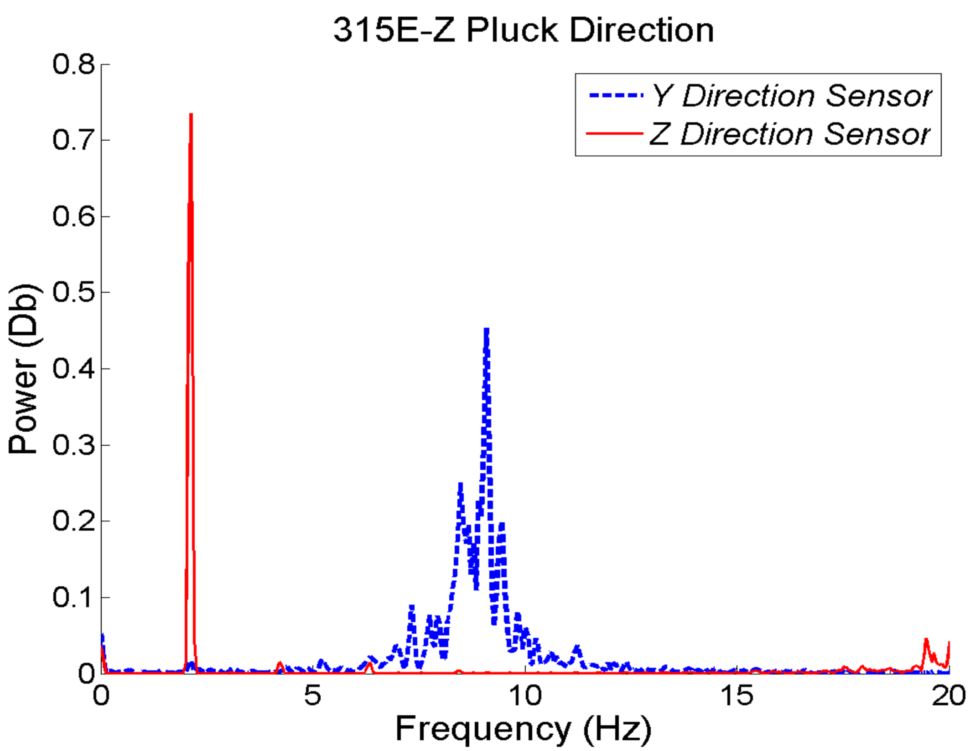
315E-Z Pluck Direction
Y Direction Sensor
Z Direction Sensor
Power (Db)
Frequency (Hz)
0.8
0.7
0.6
0.5
0.4
0.3
0.2
0.1
0
5
10
15
20

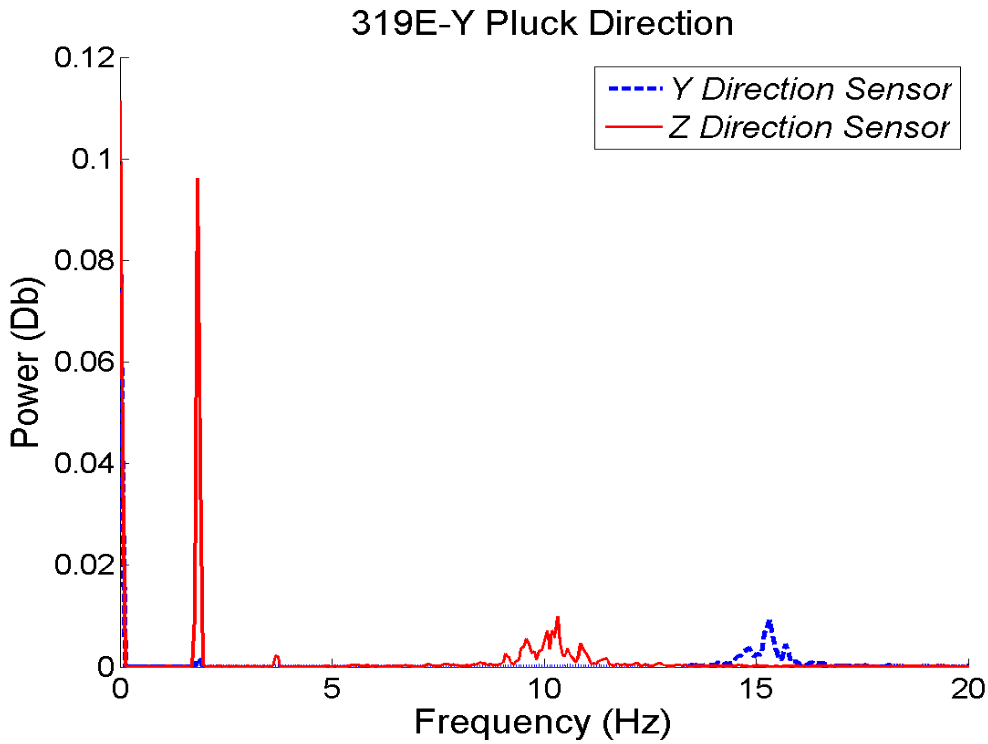
319E-Y Pluck Direction
Y Direction Sensor
Z Direction Sensor
Power (Db)
Frequency (Hz)
0.12
0.1
0.08
0.06
0.04
0.02
0
0
5
10
15
20

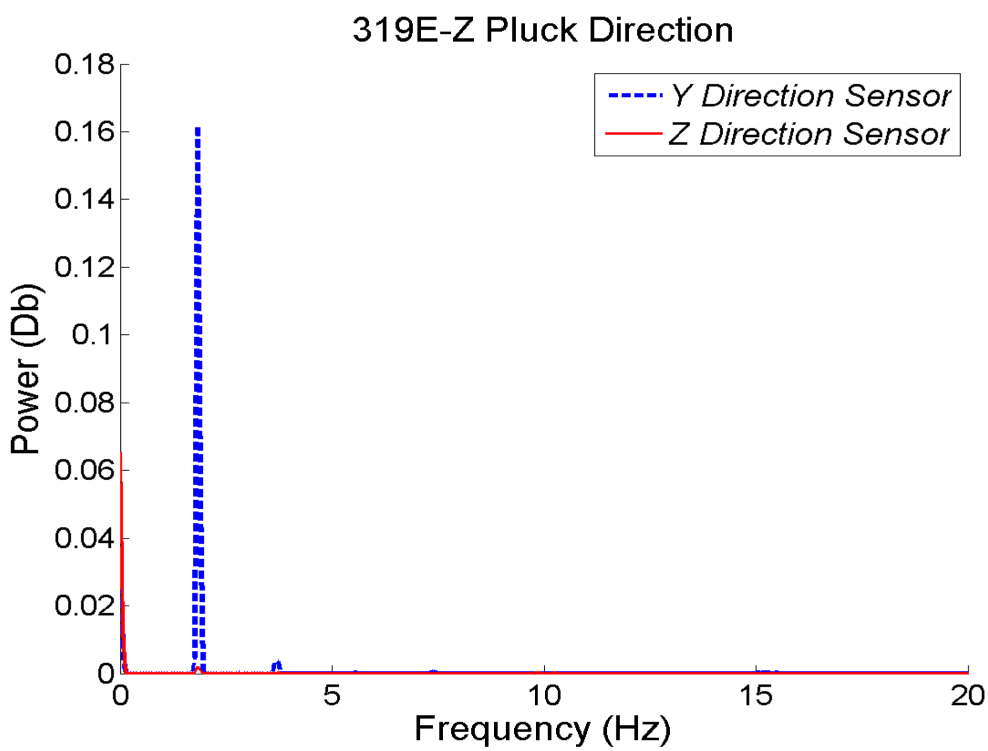
319E-Z Pluck Direction
Y Direction Sensor
Z Direction Sensor
Power (Db)
Frequency (Hz)
0.18
0.16
0.14
0.12
0.1
0.08
0.06
0.04
0.02
0
0
5
10
15
20

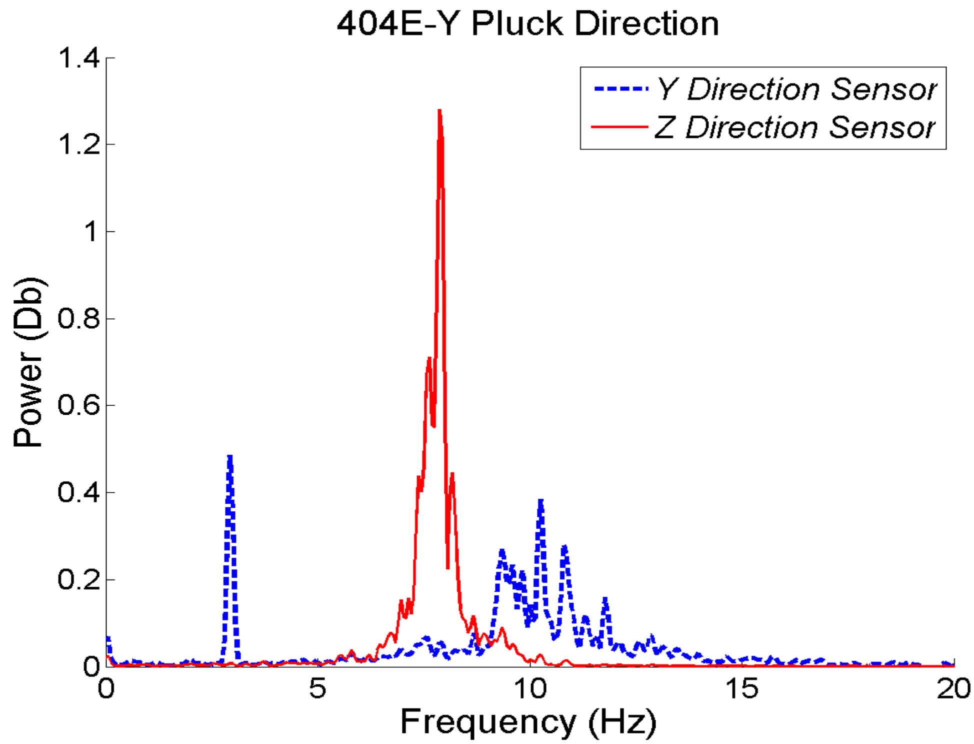
404E-Y Pluck Direction
Y Direction Sensor
Z Direction Sensor
Power (Db)
Frequency (Hz)
1.4
1.2
1
0.8
0.6
0.4
0.2
0
0
5
10
15
20

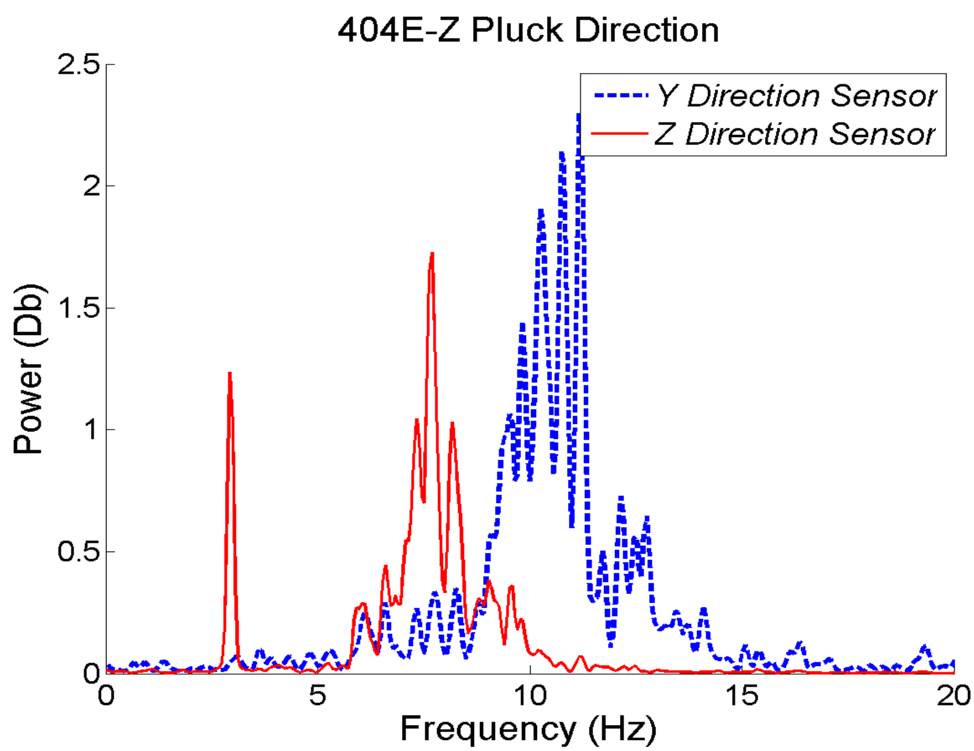
404E-Z Pluck Direction
Y Direction Sensor
Z Direction Sensor
Power (Db)
Frequency (Hz)
2.5
2
1.5
1
0.5
0
0
5
10
15
20

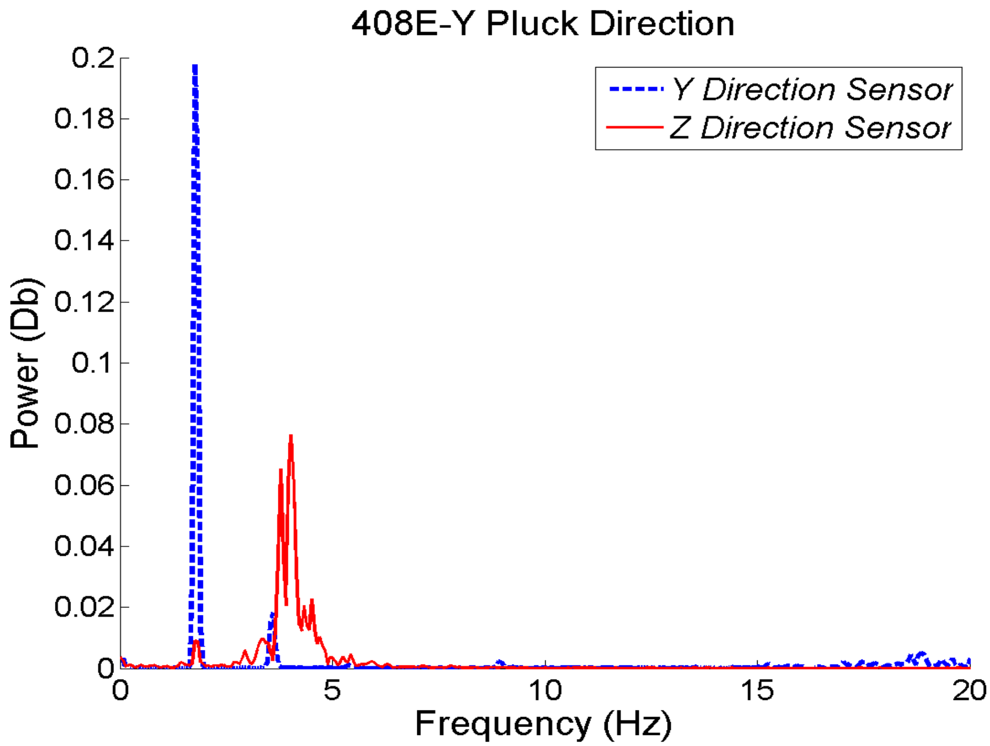
408E-Y Pluck Direction
Y Direction Sensor
Z Direction Sensor
Power (Db)
0.2
0.18
0.16
0.14
0.12
0.1
0.08
0.06
0.04
0.02
0
0
5
10
15
20
Frequency (Hz)

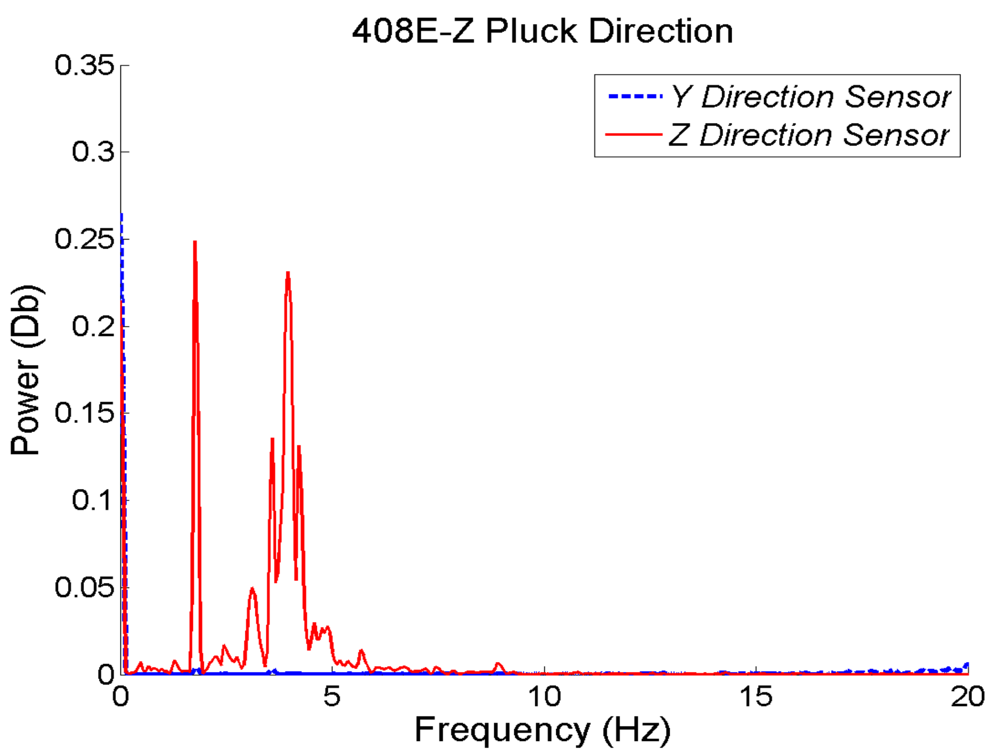
408E-Z Pluck Direction
Y Direction Sensor
Z Direction Sensor
Power (Db)
0.35
0.3
0.25
0.2
0.15
0.1
0.05
0
0
5
10
15
20
Frequency (Hz)

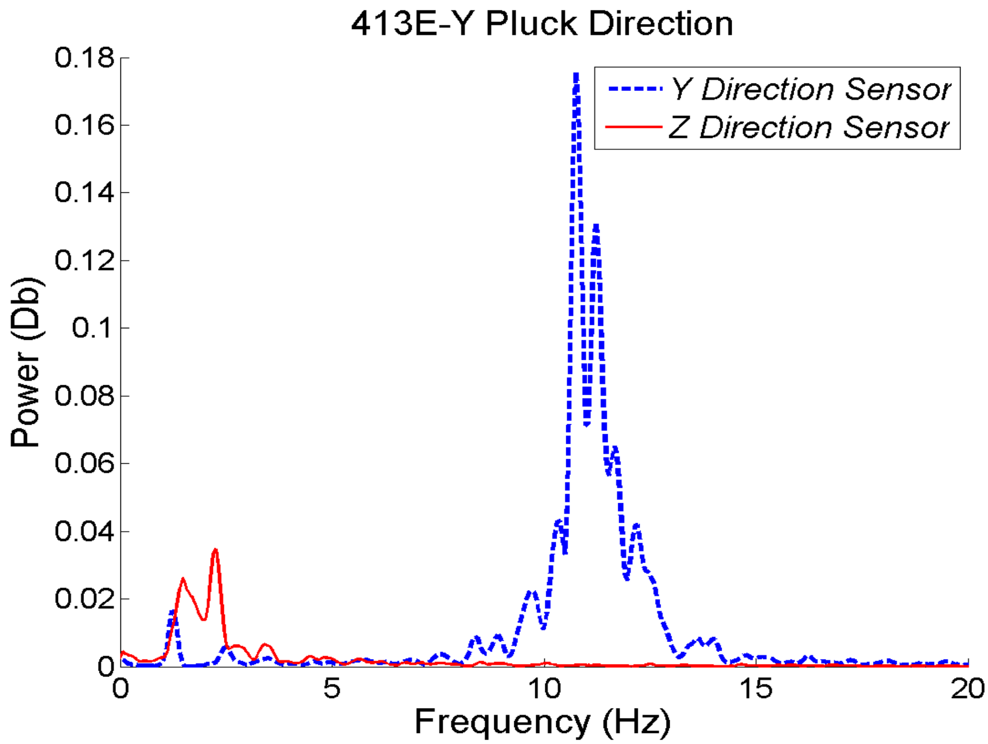
413E-Y Pluck Direction
Y Direction Sensor
Z Direction Sensor
Power (Db)
0.18
0.16
0.14
0.12
0.1
0.08
0.06
0.04
0.02
0
0
5
10
15
20
Frequency (Hz)

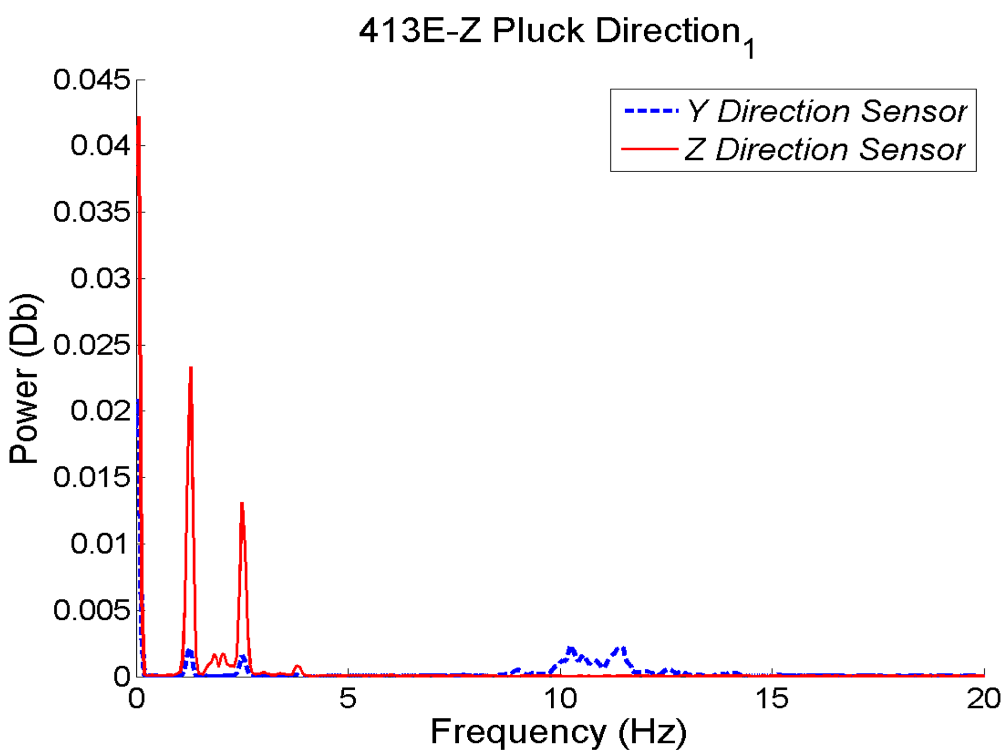
413E-Z Pluck Direction1
Y Direction Sensor
Z Direction Sensor
Power (Db)
0.045
0.04
0.035
0.03
0.025
0.02
0.015
0.01
0.005
0
0
5
10
15
20
Frequency (Hz)

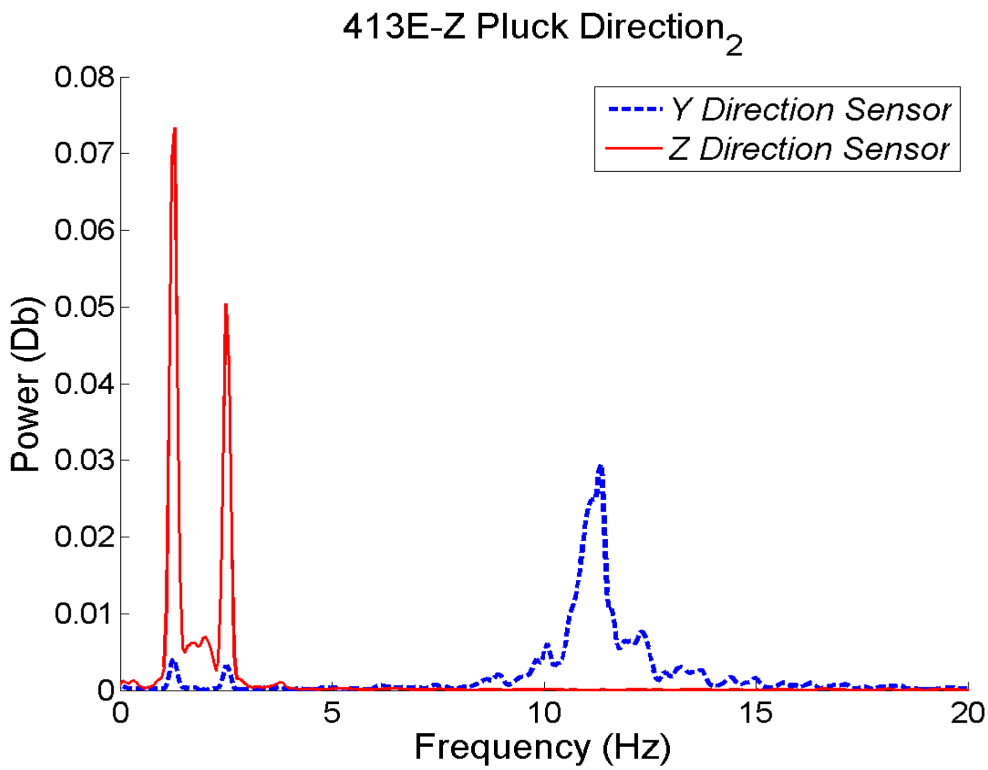
413E-Z Pluck Direction2
Y Direction Sensor
Z Direction Sensor
Power (Db)
Frequency (Hz)
0.08
0.07
0.06
0.05
0.04
0.03
0.02
0.01
0
0
5
10
15
20

Appendix B

MATLAB CODE

```
%**MASTER COPY FROM INDIAN RIVER INLET BRIDGE CABLE TENSION
ESTIMATION**

%KENT DAVIDSON
%FILE READS AND MATCHES ACCLEROMETER LOCATIONS FOR ANY TYPE OF TEXT
FILE
%WITH HEADER. PERFORMS CPSD OF DATA AND LETS USER PICK PEAKS FROM
PLOTTED
%CPSD DATA. CALCULATES ESTIMATED TENSIONS FROM USER FOUND
FREQUENCIES/

clear
clc

fileToRead1 = uigetfile('*.txt');

newData1 = importdata(fileToRead1);
% Create new variables in the base workspace from those fields.
vars = fieldnames(newData1);
for i = 1:length(vars)
    assignin('base', vars{i}, newData1.(vars{i}));
end
%CABLE ACCLEROMETER INDICATORS
names =
{'A_YE6','A_ZE10','A_YE7','A_ZE11','A_YW2','A_ZW4','A_YE8','A_ZE12','
A_YE9','A_ZE13','A_YW3','A_ZW5','A_YE10','A_ZE14','A_YE11','A_ZE15','
A_YE12','A_ZE16','A_YE13','A_ZE17','A_YE14','A_ZE18'};
[rows cols] = size(textdata);

%CONVERTS TEXT FILE TIMESTAMP AND CALCULATES AVERAGE SAMPLING
FREQUENCY
TS1 = datevec(textdata(3,1))-datevec(textdata(2,1));
TS2 = datevec(textdata(15,1)) - datevec(textdata(14,1));
TS3 = datevec(textdata(rows,1))- datevec(textdata(rows-1,1));
TAVE = (TS1+TS2+TS3)/3;
fn = round(1/TAVE(1,6));

%FINDS AND MATCHES ACCELEROMETER DATA TO COLUMNS IN DATA FILES
for i = 1:22
    TF = strcmp(textdata(1,:), names(i));
    locs = find(TF);
```

```
    accellocs(:,i) = data(:,locs);
    TF = zeros(1,cols);
end

%DEMEANS DATA FROM ACCELLOCS
for j = 1:22
    demeanaccel(:,j) = accellocs(:,j) -mean(accellocs(:,j));
end

%CPSD FOR DEMEANED ACCELEROMETER DATA
overlap = 2^10;
nfft = 2^11;
for k = 1:22
[Pxy(:,k) f] =
cpsd(demeanaccel(:,k),demeanaccel(:,k),[],overlap,nfft,fn);
end

headers =
{'219E','319E','319W','315E','310E','310W','305E','404E','408E','413E
','419E'};
%PLOT DEMEANED ACCELERATION DATA AND CPSD FOR EACH CABLE

%INSTRUCTIONS FOR SELECTING AND POPULATING FREQUENCY MATRIX
disp('The function will plot the power spectra of each cable one at a
time.')
disp('The plot will be used to find the frequencies used to calculate
tensions.')
disp('The program will prompt "Highest Estimated Mode Number", enter
the highest mode number that you want to record')
disp('If the mode that you are entering does not have a frequency
assosicated enter 0.')
disp('For example if power spectra returns the 2nd, 4th, and 6th
modes the')
disp('"Highest Estimated Mode Number" entry is 6. The entry would
look like')
disp(' 0 2nd Mode Freq 0 4th Mode Freq 0 6th Mode Freq')

%PRINTS SAMPLING RATE | SAMPLE OVERLAP | FFT WINDOW LENGTH
fprintf('Sampling Rate: %f Hz || Sample Overlap: %f || Window Length:
%f\n',fn,overlap,nfft)

%PREALLOCATION VARIABLES FOR FREQUENCY FINDING AND ORGANIZING
count = 0;
g = zeros(11,10);
cablestrings = char(headers);

for l = 1:2:21
    %PLOTS THE CPSD OF THE VARIOUS SENSORS AND ALLOWS USER TO USE
DATA
    %SWEEPER TO FIND AND PICK OUT PEAKS FOR PLOTTED DATA
    hold on
```

```
    plot(f,Pxy(:,l), 'r')
    plot(f,Pxy(:,l+1),'b')
    legend('Y-Sensor','Z-Sensor');
    if l == 1
        title(headers(1,l));
    else
        title(headers(1,round(l/2)));
    end
    xlabel('Frequency (Hz)');
    ylabel('Power');
    pause
        fprintf('Cable Number is %c%c%c%c\n\n',
cablestrings(round(l/2),1:4))
        peaknums1 = input('Number of Peaks: ');
        if peaknums1 == 0
            g(round(l/2),:) = 0;
        else
            for p = 1:peaknums1
                g(round(l/2),p) = input('Frequency: ');
            end
        end
    close
end

%FINDS THE FREQUENCIES AND REDUCES THE G MATRIX
[row col] = find(g);
colfind = max(col);

%CABLE PARAMETERS NEEDED FOR DYNAMIC CABLE THEORY
L = [505, 505, 505, 407.4, 287, 287, 171.7, 154.8, 246.6, 367.3,
458.9];
m = [1.47528, 1.47528, 1.47528, 1.008108, 0.885168, 0.885168, 0.6147,
0.590112, 0.811404, 0.934344, 1.499868];

T = zeros(11,colfind); %SPEED PREALLOCATION MATRIX METHOD
%USES CABLE PARAMETERS AND FREQUENCIES FROM ABOVE TO FIND THE
ESTIMATED
%TENSION USING DYNAMIC CABLE THEORY
for freqs = 1:11
    for d = 1:colfind
        T(freqs,d) = 4*(L(1,freqs))^2 *(g(freqs,d)/(d))^2*m(1,d);
    end
    %FINAL COLUMN IN THE MATRIX IS THE AVERAGE OF THE TENSIONS FOR
THAT
    %CABLE
    T(freqs,colfind+1) = mean(T(freqs,:));
end

N = colfind;
fprintf('The highest estimated mode number is: %1.0f\n',N);
disp('          Calculated Tensions')
```

```
fprintf('The first %1.0f number of columns are the calculated
tensions from input frequencies\n',N)
fprintf('The final column in the matrix is the average tension for
each row\n\n')
disp(T)
```